Crack development in transverse loaded base-restrained reinforced concrete walls

M. Micallef[a], R.L. Vollum[a,*], B.A. Izzuddin[a]

[a] Imperial College London, London, United Kingdom
* Corresponding author. Tel.: +44 (0) 20 75945992. E-mail address: r.vollum@imperial.ac.uk (R.L. Vollum).

Abstract

The prediction and control of crack widths in reinforced concrete structures has been the subject of research for many years. However, there is still a lack of consensus on the design of reinforcement for crack control in walls with edge restraint. The paper describes an experimental programme undertaken to investigate the influence of early-age thermal contraction and long-term shrinkage on cracking in four edge-restrained reinforced concrete walls loaded in bending about their major axis. Bending was introduced as a result of initial preload as well as restraint of deflection due to volumetric change. The walls measured 3500 mm long by 180 mm thick with heights of 500 mm and 750 mm. The paper highlights the main findings of the experimental programme and presents the results of nonlinear finite element analysis that was carried out to investigate the effects of wall geometry and reinforcement ratio on crack widths in edge-restrained walls. Results suggest that crack widths in edge-restrained walls are significantly influenced by the wall geometric properties such as wall aspect ratio and wall height which are only indirectly accounted for through the restraint factor in crack width calculations to EN 1992.

Keywords

Reinforced concrete walls; edge restraint; early-age thermal; long-term shrinkage; crack width; crack spacing; laboratory tests; numerical modelling.

Notations

c	-	cover to longitudinal reinforcement
f_{ct}	-	concrete tensile strength
f_{cm}	-	mean concrete cylinder compressive strength
f_{cu}	-	measured concrete cube compressive strength
f_{yk}	-	characteristic yield strength of steel reinforcement
h	-	wall thickness
h_e	-	element size
s_{av}	-	average crack spacing
s_{max}	-	maximum crack spacing
s_{min}	-	minimum crack spacing
w_{max}	-	maximum crack width
y	-	vertical distance from neutral axis of wall uncracked section
A_{ct}	-	area of concrete in tensile zone
A_s	-	area of tension reinforcement
E_c	-	elastic modulus of concrete
E_s	-	elastic modulus of steel reinforcement
G_f	-	fracture energy
H	-	wall height
L	-	wall length
R	-	external restraint factor
R_a	-	degree of restraint after cracking
R_b	-	degree of restraint before cracking

$\propto_t$ - coefficient of thermal expansion

$\boldsymbol{\delta}$ - measured deflection

ε_{free} - free strain in unrestrained member

ε_R - restrained strain

ε_{total} - total strain

ε_u - ultimate concrete tensile strain

$\mu\varepsilon$ - microstrain = 1 x 10^{-6} mm/mm

ν - Poisson's ratio

ρ - steel ratio based on area of concrete in tension ($= A_s/A_{ct}$)

$\Delta\varepsilon_r$ - strain induced by stage 1 loading

$\Delta\varepsilon_{max}$ - calculated extreme fibre strains induced by stage 1 loading

$\emptyset$ - reinforcement bar diameter

1. Introduction

Following casting, concrete experiences volumetric changes due to early-age thermal (EAT) strain, early-age (EA) autogenous shrinkage and long-term (LT) drying shrinkage. Restraint of free volumetric contraction induces tensile stress which can cause cracking. Unless controlled by sufficient reinforcement, cracking adversely affects durability, aesthetics and water tightness resulting in great cost to the construction industry [1]. This paper focuses on cracking in edge-restrained reinforced concrete (RC) walls and is of relevance to the design of water resisting and retaining walls cast on stiff bases.

Previous experimental studies of cracking in edge-restrained RC walls are limited and unrepresentative of practice due to tests being carried out on reduced-scale walls with either micro-concrete and reduced bar diameters [2] or mortar mixes [3-5]. Where extensive

monitoring of field walls has been carried out [4, 5], available information is incomplete. This paper develops an improved understanding of cracking in RC edge-restrained walls on the basis of laboratory tests and nonlinear finite element analysis (NLFEA).

Cracking in RC walls with edge restraint is much less researched than cracking in end-restrained members and as yet there is no consensus on the mechanism of crack control in edge-restrained members [6]. A key difference between edge and end restraint is that axial force is constant along the length of end-restrained members but not edge-restrained members where cracking occurs at locations of high restraint. It is convenient to define the degree of restraint in terms of a restraint factor *R* calculated as follows:

$$R = \frac{\varepsilon_{free} - \varepsilon_{total}}{\varepsilon_{free}} \qquad \text{(equation 1)}$$

where ε_{free} and ε_{total} are the free and total strains respectively.

Research [7, 8] shows that restraint is greatest at the centre and near the base of edge-restrained walls, with restraint decreasing vertically with height from the base and horizontally with distance from the wall centreline.

Stoffers [2] investigated shrinkage induced cracking in edge-restrained RC walls. He examined linear elastic stress distributions in walls constrained to remain straight and showed that tensile stresses (resulting from restraint) only develop in the upper edge of walls with aspect ratios greater than 1.5. He tested micro-concrete walls measuring 375 mm high by 60 mm thick with aspect ratios L/H of 6.7 and 8 that were either constrained to remain straight or free to curve on contraction. In walls constrained to remain straight, crack widths increased with height from the base with the largest crack widths occurring at the top of the wall where crack spacing was greatest. Reinforcement had a greater effect on crack widths in walls constrained to remain straight than walls free to curve where curvature induced compressive

flexural stresses in the upper part of the wall. In his free to curve walls, Stoffers observed crack widths to increase up to a height of approximately 200 mm from the base and then decrease with increasing height from the base.

Kheder and his co-workers [3-5] showed that crack widths in edge-restrained walls are proportional to the change in restraint on cracking defined as $R_b - R_a$ where R_b and R_a denote the elastic restraint factors before and after cracking. Kheder [5] used two-dimensional (2D) elastic finite element analysis (FEA) to show that $R_b - R_a$ increases with wall aspect ratio. He also developed idealised diagrams of $R_b - R_a$ for the calculation of crack width. He [5] concluded that where possible, walls should be constructed with aspect ratios between 1 and 3 to reduce the amount of reinforcement required for crack control. Kheder also observed crack widths in base-restrained walls of the same aspect ratio to increase with wall height [3-5]. Consequently, the reinforcement ratio required for crack control in walls of the same aspect ratio increases with wall height. Correlation is also observed between the location of maximum EAT crack width and maximum temperature drop [9, 10].

Experimental and field data from studies described in this section led researchers to propose equations for estimating crack widths in edge-restrained RC walls. Notably, the equations of Stoffers [2] and Kheder [3-5] include wall height and aspect ratio in the calculation of crack spacing unlike the superseded UK code BS 8007 [11] and EN 1992 [12, 13].

2. Experimental details

2.1 Introduction

As previously discussed, very limited experimental and field data are available on cracking in edge-restrained RC walls. To this end, the authors tested four edge-restrained walls (E-W1 to

E-W4) in the Structures Laboratory of the Department of Civil and Environmental Engineering at Imperial College London [14]. In order to simulate a wall constrained to remain straight, vertical deflections due to concrete volumetric change were restrained as described in Section 2.5. The lateral forces induced by vertical restraint caused bending to develop in the walls. Additionally, transverse preload was applied to ensure subsequent restraint induced cracking. The preload compensated for the flexibility of the vertical restraint and, in the case of walls E-W1 to E-W3 was sufficient to cause immediate cracking. Consequently, tests E-W1 to E-W3 examined the effect of volumetric change on walls pre-cracked in bending. However, the majority of cracks formed in all walls due to restrained shrinkage. The walls were monitored for a minimum of two months for EAT and LT shrinkage cracks. The average air temperatures varied between 20 °C and 27 °C, and the relative humidity between 40 % and 60 % over the duration of the test programme. The test results are used to develop an improved understanding of EAT and LT cracking in edge-restrained walls and to validate NLFEA models, which are subsequently used to carry out parametric studies of variables not considered in the laboratory tests.

2.2 Testing arrangement

The test setup (Figure 1) consisted of a RC wall cast against a hot rolled steel universal column (UC), which provided edge restraint. A steel section was chosen for edge restraint because steel, unlike concrete, is not subject to creep or shrinkage. The clearly defined restraint condition simplified data interpretation as well as NLFEA modelling (described in Section 3.3). A 150 mm kicker was cast onto the UC at least one week prior to casting the wall above to simulate the boundary conditions of a wall cast onto a concrete base. The kicker increased the base restraint provided by the UC and reduced heat losses through the

UC. The kicker was connected to the UC by pairs of 19 x 100 mm shear connectors at a close spacing of 100 mm chosen to minimise slip between the UC and kicker.

a)

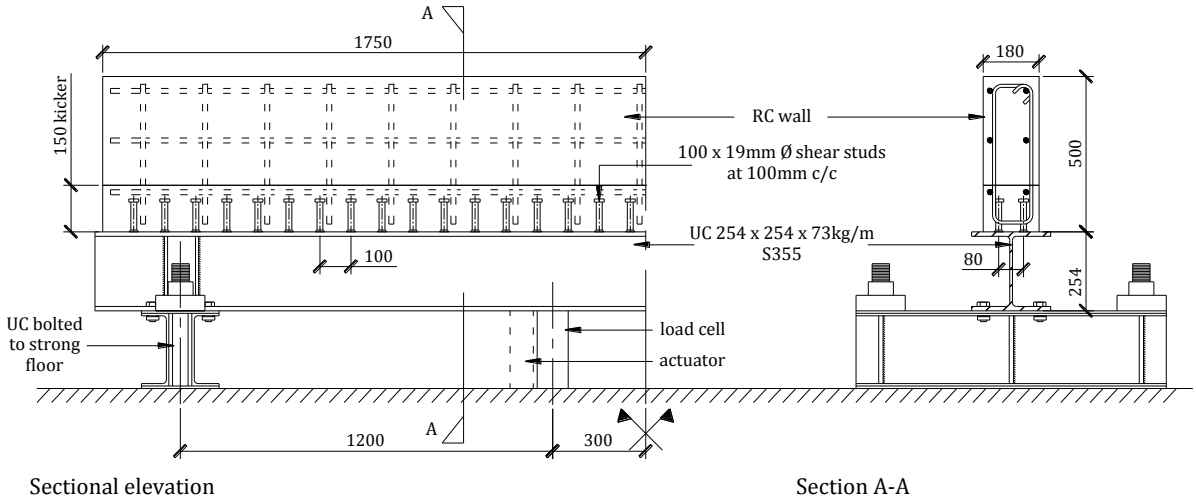

b)

Figure 1: The experimental wall setup: a) elevation and transverse section of a 500 mm high wall (E-W3); and b) view of the experimental setup (All dimensions are in mm)

2.3 Design of specimens

Key design requirements were that the walls needed to be sufficiently long for multiple cracks to develop and the restraining UC stiff enough to cause cracking. Walls E-W1 and E-W2 measured 3500 (L) x 180 (h) x 750 mm (H) giving an aspect ratio above the kicker of 5.8, which is well within the practical range of 1 to 8 identified by Kheder [5]. A 254 x 254 x

73 UC was adopted for base restraint on the basis of parametric studies. The depth, cross-sectional area and major axis second moment of area of the UC are 254.1 mm, 93.1 cm^2 and 11407 cm^4. The height of walls E-W3 and E-W4 was reduced to 500 mm, which corresponds to an aspect ratio above the kicker of 10, in order to increase restraint. A wall thickness h of 180 mm was adopted because it was wide enough to accommodate four layers of reinforcement yet fit neatly onto the top flange of the restraining UC section leaving sufficient space to support the shuttering.

The walls were reinforced vertically using 10 mm diameter bars spaced at 200 mm centres in each face and horizontally with 12 mm diameter bars at centres of either 200 mm (E-W1, E-W2 and E-W3) or 100 mm (E-W4) (Table 1 and Figure 2). Walls E-W1 and E-W2 were identical apart from the concrete mix design. Reinforcement detailing was similar to that used in RC retaining walls where vertical bars are placed in the outside layer on the earth face and the inner face on the exposed face [15]. Consequently, the concrete cover to the horizontal reinforcement differed on each face of the wall. Additionally, two 1000 mm long control specimens (one reinforced and one unreinforced) with the same cross-section as walls E-W1 and E-W2 were cast to assess free EAT strain and drying shrinkage.

Table 1: Details of tested walls

wall notation	**concrete mix design**	**horizontal bar diameter [mm]**	**horizontal bar spacing [mm]**	**concrete cover – face 1 [mm]**	**concrete cover – face 2 [mm]**	**RC wall height [mm]**
E-W1	1	12	190	15	30	750
E-W2	2	12	190	15	30	750
E-W3	2	12	170	15	30	500
E-W4	2	12	85	15	25	500

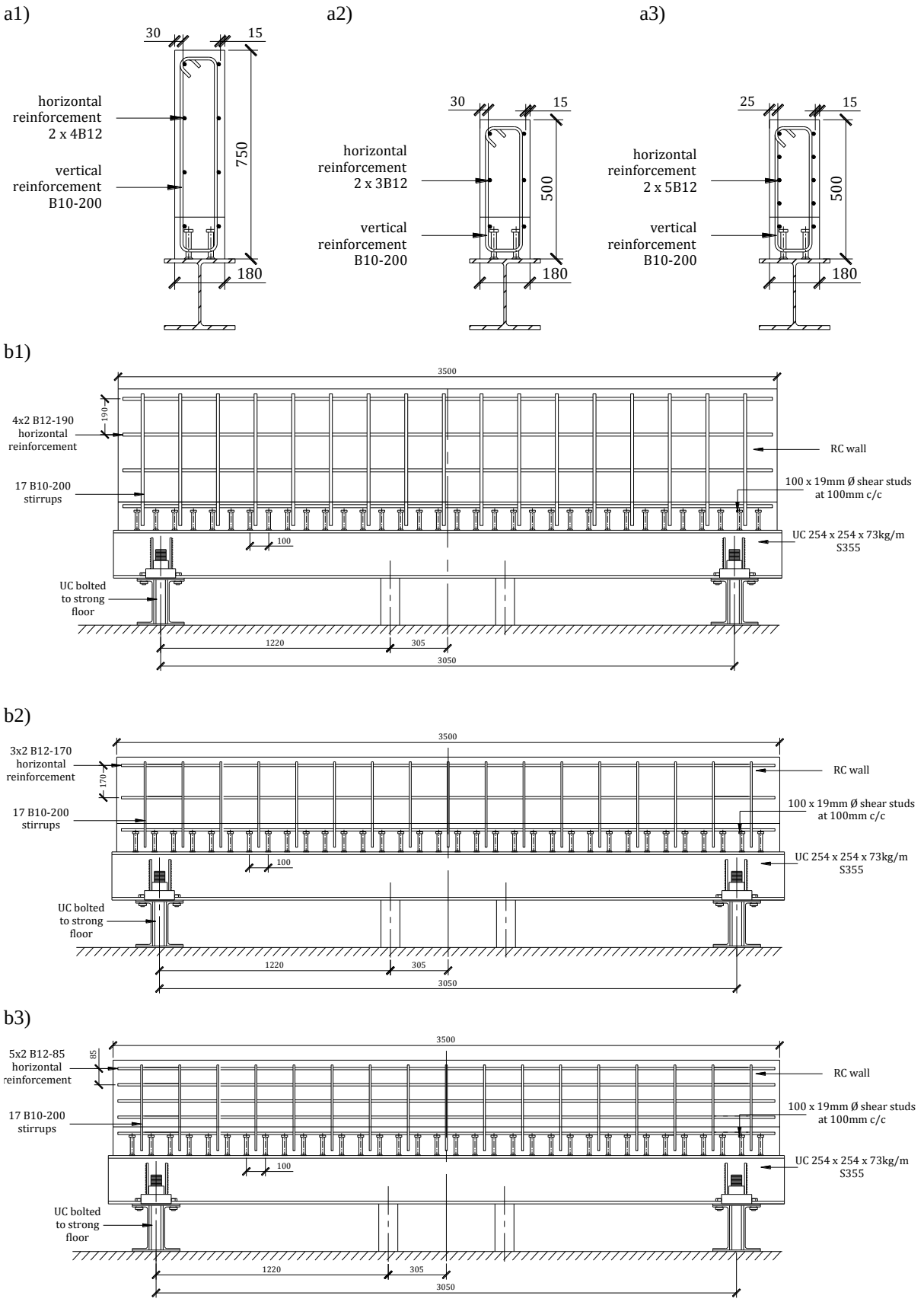

Figure 2: Reinforcement arrangement in edge-restrained wall specimens: a) cross-section for 1) E-W1 and E-W2; 2) E-W3; and 3) E-W4; and b) sectional elevation for 1) E-W1 and E-W2; 2) E-W3; and 3) E-W4 (All dimensions are in mm)

2.4 Material properties and instrumentation

Two concrete mixes were used. Both had a very high cement content of 500 kg/m^3 in order to maximise the peak hydration temperature. The mix design for E-W1, hereinafter referred to as mix 1, had a water cement ratio of 0.45. In order to get the desired slump of approximately 175 mm and high shrinkage strains, a high fine (with 60 % passing the 600 μm sieve) to coarse (10 mm maximum size) aggregate ratio of 75 % was used. Calorimeter results showed the peak temperature not to vary significantly with water cement ratio for the same cement content. Therefore, the water to cement ratio was increased to 0.53 in mix 2, used in E-W2, E-W3 and E-W4, to decrease the concrete tensile strength and hence, promote cracking. The maximum temperatures reached were as high as 70 °C in E-W1 and E-W2 and 60 °C in E-W3 and E-W4 as shown in Figure 3 where "m" depicts temperatures at mid thickness of the wall and "c" depicts temperatures at a depth of 25 mm from the wall surface. The temperature variation was minimal throughout the wall length and thickness as shown in Figure 3.

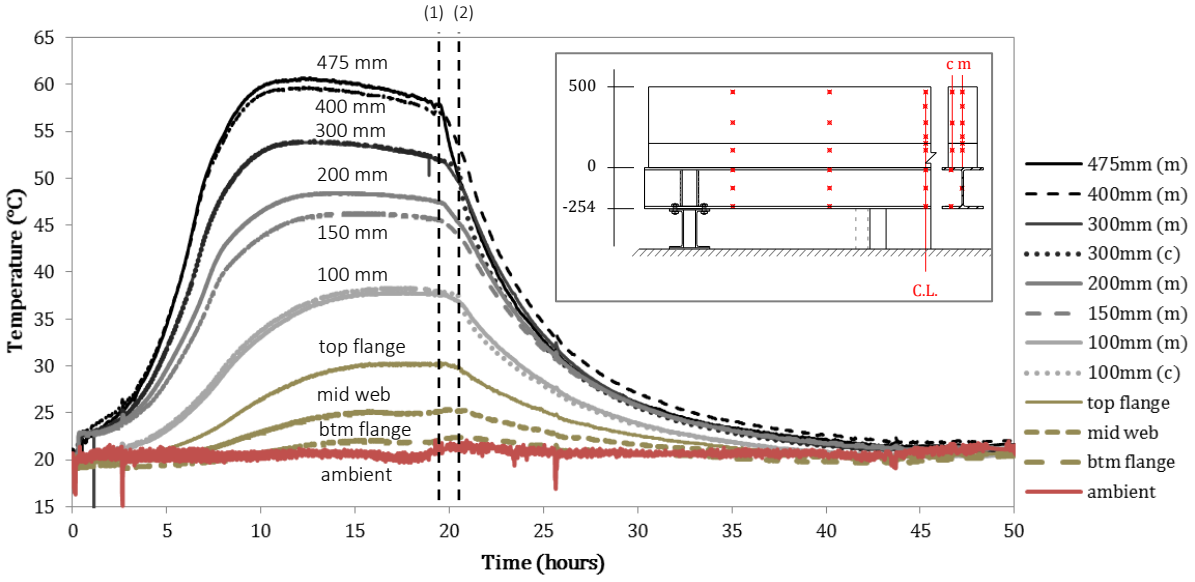

(1) – removal of first forwork face
(2) – removal of second forwork face

Figure 3: Typical temperature variations with time from casting at the wall centreline and at different wall heights (E-W4)

a)

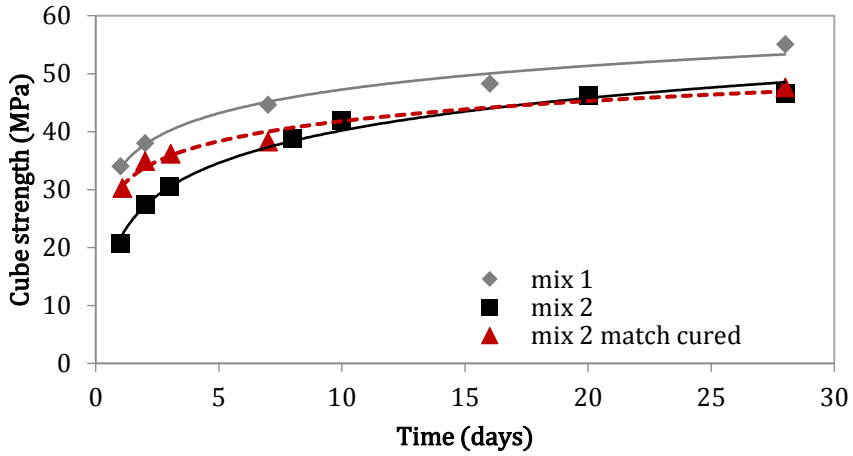

b)

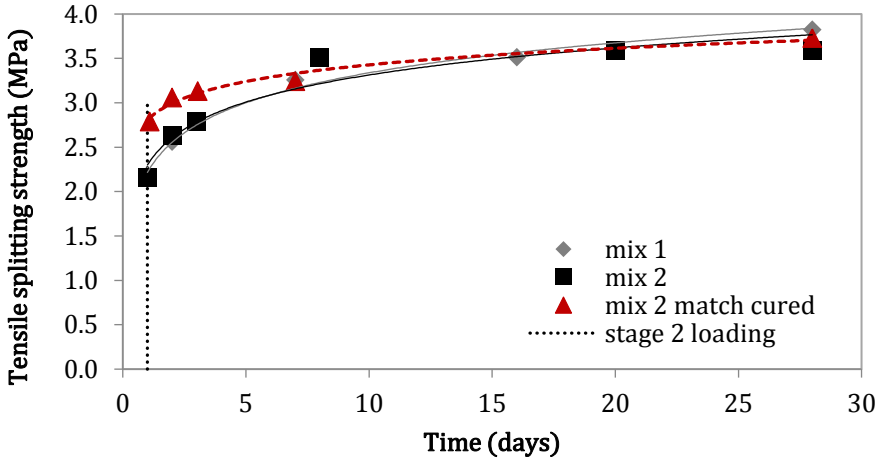

Figure 4: Average concrete strengths for mix 1 (E-W1) and mix 2 (E-W2 to E-W4): a) compressive cube strength; and b) tensile splitting strength

Figure 4 shows the concrete compressive and tensile strength development with time for both mixes. Strengths are shown for control specimens cured in water at 20° C. Additionally, temperature match cured cube strengths are shown in Figure 4a for mix 2. Compressive strengths were determined from 100 mm cubes and tensile strengths from splitting tests on cylinders of 100 mm diameter and 250 mm height. Regression analysis was used to determine the following relationship between the tensile and compressive strength for the water cured specimens of mix 2.

$$f_{ct} = 0.315 f_{cu}^{0.64} \qquad \text{(equation 2)}$$

Equation (2) was then used to estimate the insitu tensile strength within the wall as a function of time. The resulting strengths are plotted in Figure 4b.

The concrete elastic modulus and Poisson's ratio of mix 2 remained sensibly constant between 3 days and 28 days during which time their average values were 31.9 GPa and 0.17 respectively. The coefficient of thermal expansion was estimated as 11.8 με/°C from strains measured in unrestrained control walls.

As illustrated in Figure 5, the instrumentation included:

- type K exposed welded tip thermocouples (denoted "T") measuring temperature in the concrete, UC and air;
- YFLA-5-1L electrical strain gauges (denoted "S") measuring strain in the UC;
- 100 mm linear variable differential transformers (LVDTs) (denoted "D") measuring displacements;
- Demountable mechanical (DEMEC) strain gauge studs fixed in a square grid of 150 mm measuring surface strain.

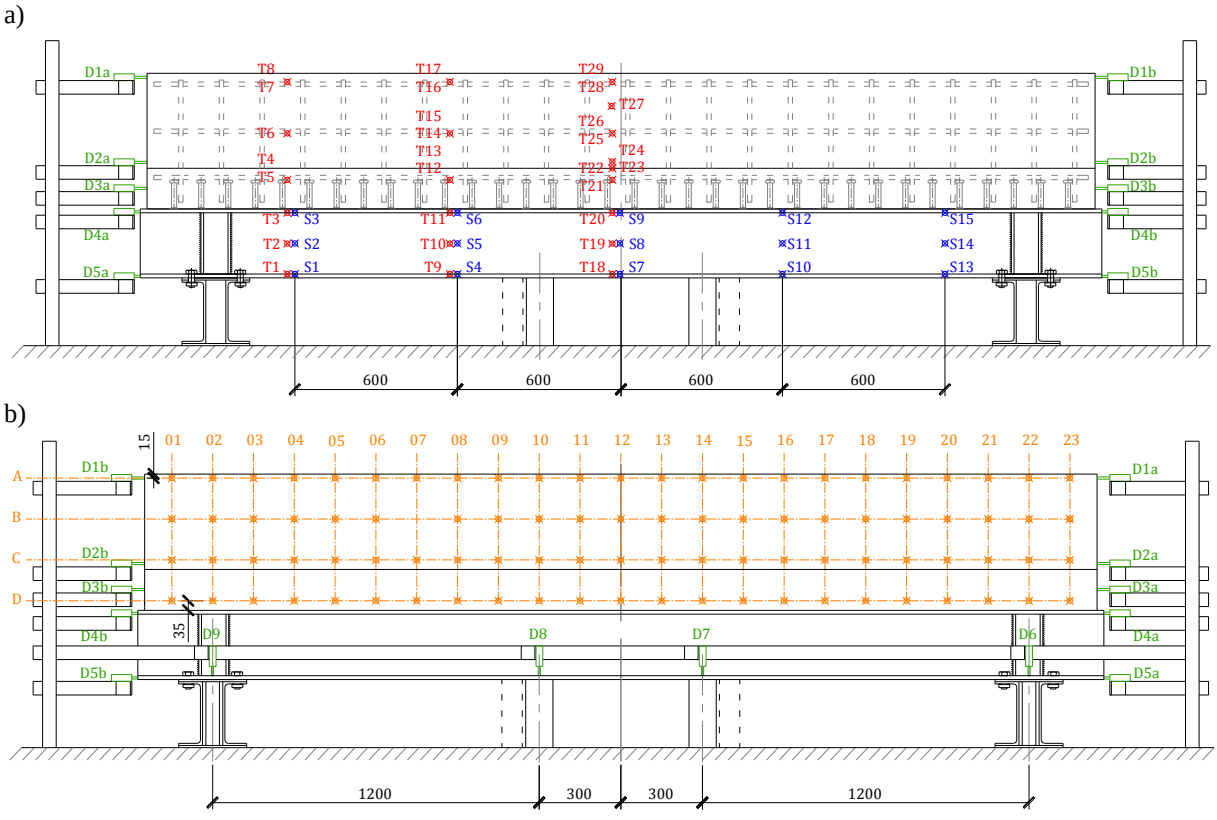

Figure 5: Instrumentation setup: a) thermocouple, strain gauges and horizontal LVDTs locations; and b) horizontal and vertical LVDTs locations and DEMEC grid for E-W3 and E-W4 (All dimensions are in mm)

Detailed monitoring of each wall was carried out for a minimum of six weeks. Crack widths were measured at fixed locations, perpendicular to the crack, using a portable microscope having a x40 magnification power and precision of +/- 0.02 mm. Additionally, crack propagation was monitored photographically with time.

2.5 Testing procedure

Initially, the ends of the UC were bolted to the laboratory strong floor, to provide vertical but not axial restraint, the reinforcement was fixed and formwork erected. Subsequently, a 150 mm high concrete kicker was cast onto the UC at least one week before casting the wall. The plywood shuttering was insulated with 50 mm thick polyisocyanurate (PIR) insulation boards with thermal conductivity of 0.44 W/m2K. The PIR boards were tightly fitted between timber joists on both wall faces and ends (Figure 6). Immediately after casting, the top of the wall was also insulated with PIR insulation boards. Prior to removing the shuttering, the wall was only supported at its ends. Consequently, the wall initially deflected upwards as the concrete heated. During cooling, downwards displacement of the wall was restrained by two centrally positioned load cells placed between the steel UC beam and the laboratory strong floor. This arrangement was chosen to enable the effective restraint to be controlled through the introduction of transverse displacement. Approximately 18 to 20 hours after casting each wall, immediately before stripping the formwork, the UC was given a small vertical preload to increase the effective restraint. The preload was introduced in a carefully controlled two stage procedure. In the first stage, a small preload was applied to the beam with actuators. The screw thread on the load cell was then manually tightened to establish contact with the UC. Subsequently, the actuator was unloaded leaving a residual preload in the load cell. Load was applied with a single centrally positioned actuator in test E-W1 and with two actuators, positioned immediately adjacent to the load cells (see Figure 2), in the remaining tests. The

loading on the beam was continuously monitored during this procedure as were displacements. Table 2 shows the peak actuator loads and the initial load cell reactions immediately after unloading of the actuators.

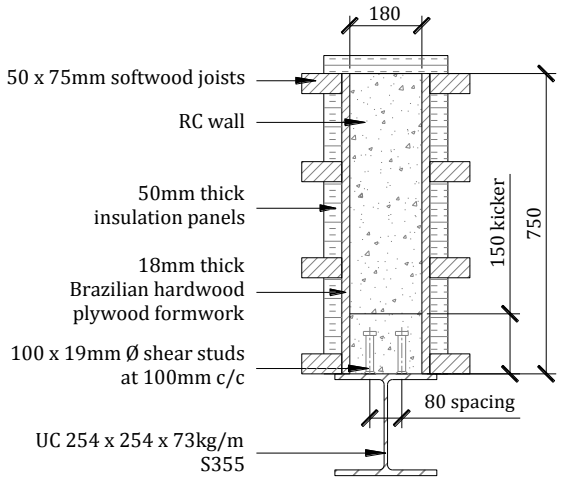

Figure 6: Insulation setup for 750 mm high edge-restrained walls (E-W1 and E-W2) (All dimensions are in mm)

Table 2: Actuator load application

wall notation	stage 1 actuator loading			stage 2 actuator loading				cooled to ambient	end of test
	time [hrs]	actuator [kN]	load cell [kN]	time [hrs]	load cell^{-}[kN]	actuator [kN]	load cell^{+} [kN]	load cell [kN)	load cell [kN]
E-W1	18.5	25	12	45	97	304	110	97	105
E-W2	19.5	27	33	22	57	90	73	103	90
E-W3	19	24	28	21	37	52	42	62	64
E-W4	19.5	25	23	n/a	n/a	n/a	n/a	66	60

- load cell reading before second stage loading
+ load cell reading after unloading the actuators

Immediately after stage 1 preloading, the formwork and insulation were removed from the ends and one face of the wall at 18.5, 19.5, 19 and 19.5 hours from casting for walls E-W1, E-W2, E-W3 and E-W4 respectively. The end transducers were installed and, over a period of around 60 to 90 minutes, DEMEC studs were fixed in the central 1000 mm width of the wall, after which initial DEMEC readings were taken. Immediately afterwards, the remaining formwork and insulation were removed at 19.5, 21, 20 and 20.5 hours from casting for walls E-W1, E-W2, E-W3 and E-W4 respectively and remaining DEMEC studs fixed.

Wall E-W1 did not crack during cooling as intended so was further loaded at the end of cooling. This induced a single crack. Due to concern that the edge restraint was insufficient to cause cracking, the stage 1 preload was increased in tests E-W2, E-W3 and E-W4. Additionally, walls E-W2 and E-W3 were subjected to a second stage of loading (Table 2) during cooling which caused initial cracking. Stage 2 loading followed the same procedure as stage 1. In E-W2 and E-W3, stage 2 loading was applied immediately after formwork had been stripped off the second face.

Cracking was monitored in each wall for around six weeks after which the walls were transversely loaded to investigate the effect of short-term loading on restraint induced cracking as well as to determine developed crack patterns. The transverse loading was applied with two actuators positioned as shown in Figure 1. Each actuator was loaded to first 125 kN and then 200 kN which was the maximum allowable.

3. Nonlinear finite element analysis

3.1 Introduction

NLFEA was validated using the test results and then used in parametric studies to investigate the influence on crack width of wall aspect ratio and reinforcement ratio. All numerical modelling was carried out with ADAPTIC [16], a NLFEA program developed at Imperial College London.

3.2 Modelling procedures

Dynamic analysis was adopted in the NLFEA since this ensured convergence following cracking. Concrete elements were discretised with 2D four-noded flat shell elements and reinforcement with elasto-plastic 2D beam-column elements. A limitation of the NLFEA is

that the influence of cover is neglected since the analysis is 2D. Two concrete material models were used – a time-dependent model ("creep"), in which creep and shrinkage are modelled, and a time-independent ("no creep") one with fixed concrete properties. The "no creep" analysis was undertaken since Kianoush et al. [20] used a similar analysis to achieve reasonable predictions of LT crack widths in base-restrained walls subject to EAT and shrinkage volumetric change.

The "creep" concrete model ("con12" [17]) utilises a fixed-crack methodology. Creep, shrinkage and the development of concrete strength and stiffness with time are calculated in terms of 28 day properties in accordance with Model Code 1990 (MC 1990) [18] which considers uncracked concrete as an ageing visco-elastic model in both tension and compression. MC 1990 calculates creep as the product of the elastic strain and a notional creep coefficient which depends on the concrete age at loading. For variable stresses or strains the principal of superposition is assumed to be valid. The relations used to calculate MC 1990 creep coefficients are empirical. In con12, the Volterra's integral equation is solved by developing the relaxation function in a series of exponential functions and applying the trapezoidal rule [19]. In cracked elements, creep is linked only to the elastic part of the total strain. Modelling of creep is simplified in the NLFEA because no differentiation is made between tensile and compressive creep. Consequently, the analysis is unable to accurately replicate crack development with time. Based on the research of Kianoush et al. [20], it was anticipated that the prediction of LT crack widths would be less affected by inaccuracies in modelling of creep. Support for this hypothesis is provided by Beeby and Scott [21] who examined loss of tension stiffening with time in RC prisms tested in tension under sustained load. They concluded that "*the major mechanism controlling the long-term loss of tension stiffening is the development with time of cumulative damage. This may be the formation or*

extension of existing surface cracks or the development or extension of internal cracks. Creep plays an insignificant part in the changes in tension stiffening with time".

A rotating-crack concrete material model ("con9" [19]) was used in the "no creep" analyses with constant concrete properties where the most significant omission is creep. Concrete is modelled as linear in compression in con9. Real time was determined in the "no creep" analysis by relating the imposed free strain to its time of occurrence in the test.

A Rankine type plasticity based tensile cut off is used in both con9 and con12. After cracking, the concrete tensile stress was assumed to reduce linearly to zero at an ultimate strain $\varepsilon_u = 2\,G_f/(f_{ct}h_e)$ where f_{ct} is the concrete tensile strength, G_f is the fracture energy calculated according to Model Code 2010 (MC 2010) [20] and h_e is the element size [21].

Bond-slip between reinforcement and concrete was modelled using a tri-linear idealisation of the MC 2010 bond-slip relationship. The modelling of bond-slip in conjunction with the very fine adopted mesh (see Figure 7) effectively simulates discrete cracks because cracks are localised in vertical columns of single elements [23]. Consequently, crack widths were calculated directly by subtracting horizontal nodal displacements of cracked elements and correcting for the displacement of uncracked concrete.

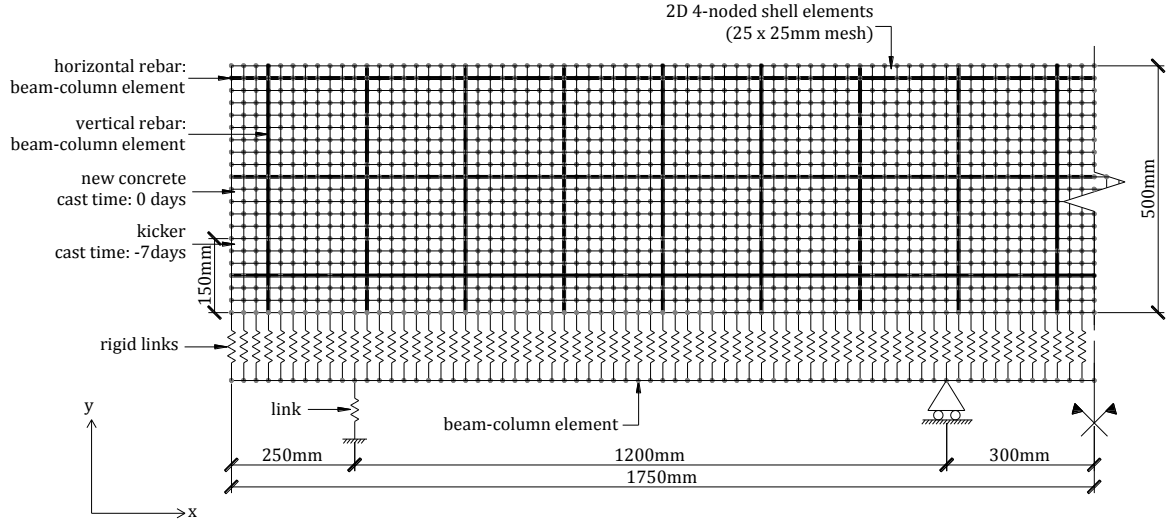

Figure 7: Representation of a NLFEA creep model of an edge-restrained experimental wall (E-W3)

3.3 Modelling experimental walls

The NLFEA was validated by modelling the tested walls with both the "no creep" and "creep" concrete models. No damping was applied in the "creep" analysis and 5% in the "no creep" analysis. Table 3 gives the 28 day concrete and reinforcement material properties used in the NLFEA. As previously described, con12 calculates concrete properties at time t in terms of the 28 day concrete cylinder strength. Consequently, the concrete compressive strengths in Table 3 are 28 day cylinder strengths calculated as 0.8 times the 28 day cube strength of mix 2. In analyses with con12 and staged loading, the concrete tensile strength was fixed at 2.7 MPa, which is the insitu tensile strength at stage 2 loading (see Figure 4b), throughout the analysis. This was done to allow for the experimentally observed reduction in concrete tensile strength under sustained load [24] which was assumed to be 25%. Figure 7 shows the finite element mesh used to model wall E-W3, which is representative. The edge-restraining UC was modelled using 2D beam-column elements. The ends of the UC were vertically restrained with link elements positioned at 250 mm from each end. The stiffness of the link elements was experimentally determined to be 400 kN/mm. At each load cell location, the UC nodes were restrained from moving vertically. The NLFEA was run both without and with the displacement induced by stage 1 and 2 actuator loading which was applied as an acceleration time history. Slip was not modelled between either the concrete and UC or the wall and kicker because measurements showed it to be minimal.

Table 3: Concrete material properties used in NLFEA of tested walls

material model	**creep modelled**	f_{cm} **[MPa]**	f_{ct} **[MPa]**	E_c **[GPa]**	G_f **[N/m]**	$\propto_t$ **[με]**	ν	f_{yk} **[MPa]**	E_s **[GPa]**
"con12"	yes	38*	3.6*	33*	140	11.8	0.17	650#	210#
"con9"	no	n/a	3.6	32	140	11.8	0.17	650#	210#

* specified at 28 days
# measured from tension tests on reinforcement bars

In the "creep" models, only half the wall length was modelled in order to minimise computational effort. Different casting times were specified for the material properties of both the kicker (negative time) and the new concrete (casting time = 0). Negative temperatures were applied to the concrete and reinforcement elements as shown in Figure 8a one day after casting the "new" concrete in order to simulate contraction due to cooling which was imposed at the rate shown in Figure 8b. The measured temperature drops were similar in all four walls (Figure 8a).

a)

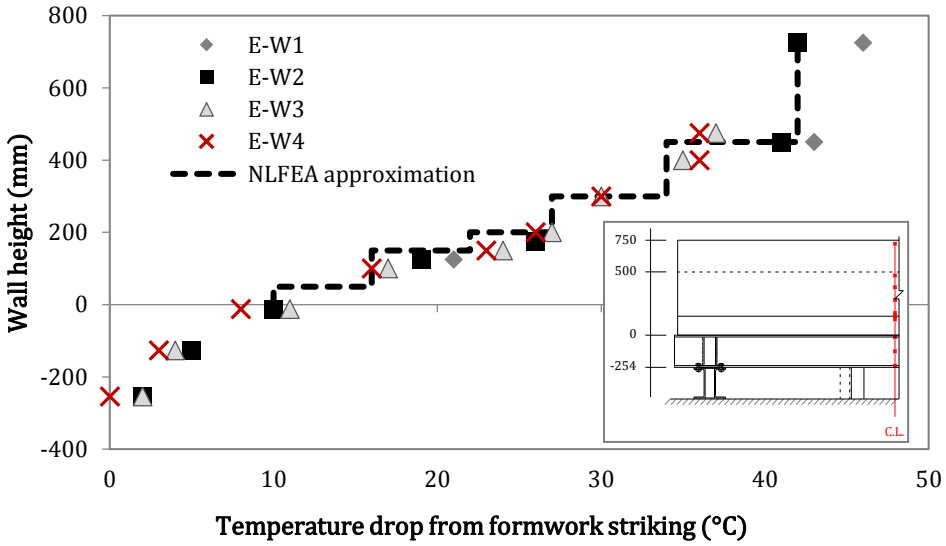

b)

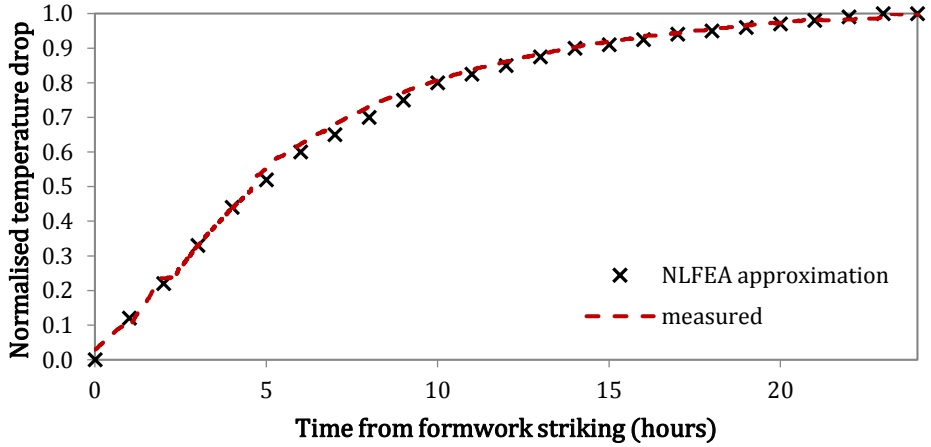

Figure 8: Measured and approximated temperatures in NLFEA validation models: a) temperature variation with wall height; and b) cooling rate with time

The full wall length was modelled in the "no creep" NLFEA which was used to calculate LT crack widths. Temperature drops were applied to the concrete and rebar elements as shown in Figure 8a. Additionally, a further uniform temperature drop of 23 °C was applied to the concrete shell elements to simulate the shrinkage strain of 280 με measured at 6 weeks (see Figure 9).

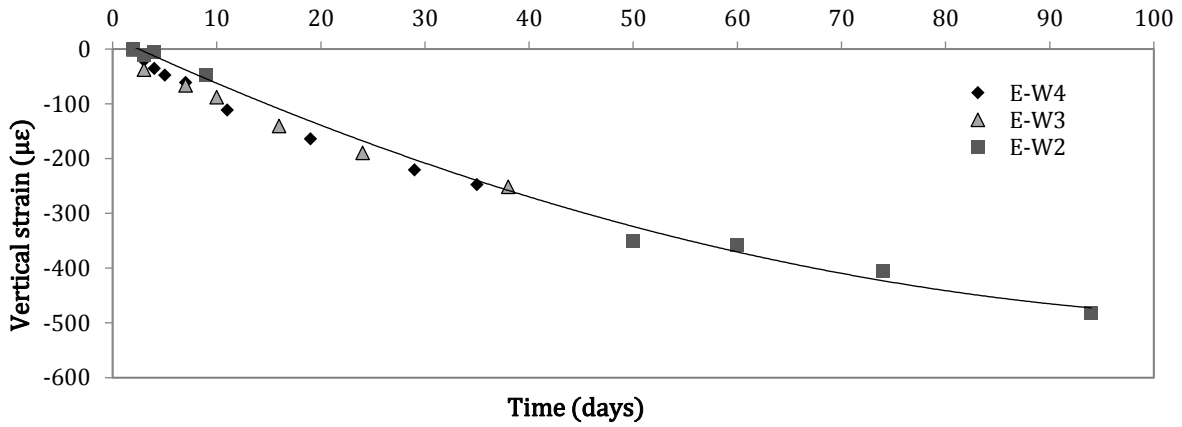

Figure 9: Shrinkage strains measured from vertical DEMEC strains and excluding EAT strains

4. Test results and analysis

This section presents the test results and makes comparisons with the NLFEA predictions. Unless otherwise stated, time is measured from casting the wall above the kicker. Full detailed results are reported by Micallef [14].

Following formwork removal, the walls contracted as they cooled causing the load cell reactions to increase (Figure 10). The measured reactions increased approximately linearly with temperature drop but remained almost constant and independent of shrinkage following cooling to ambient temperature.

a)

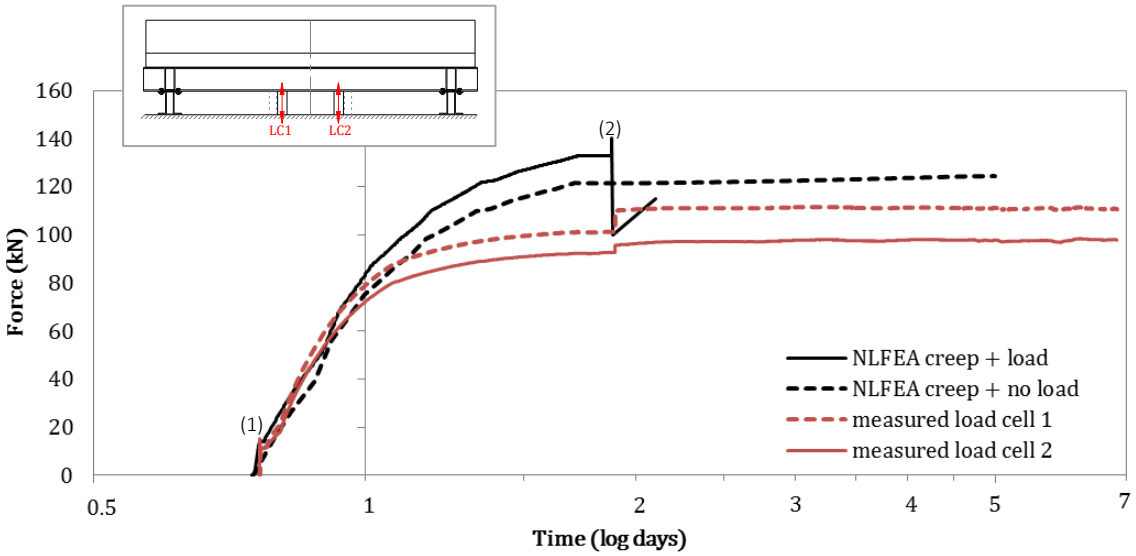

b)

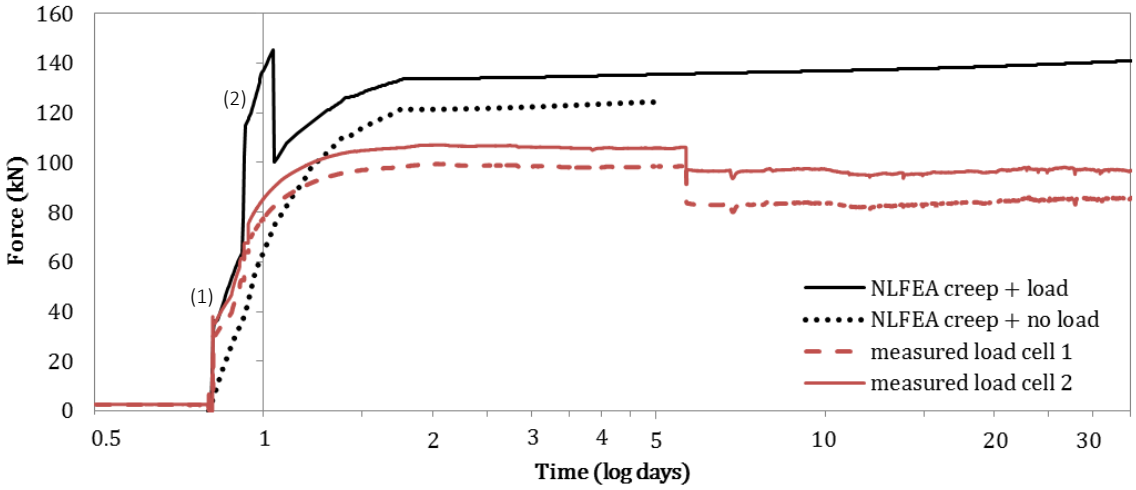

c)

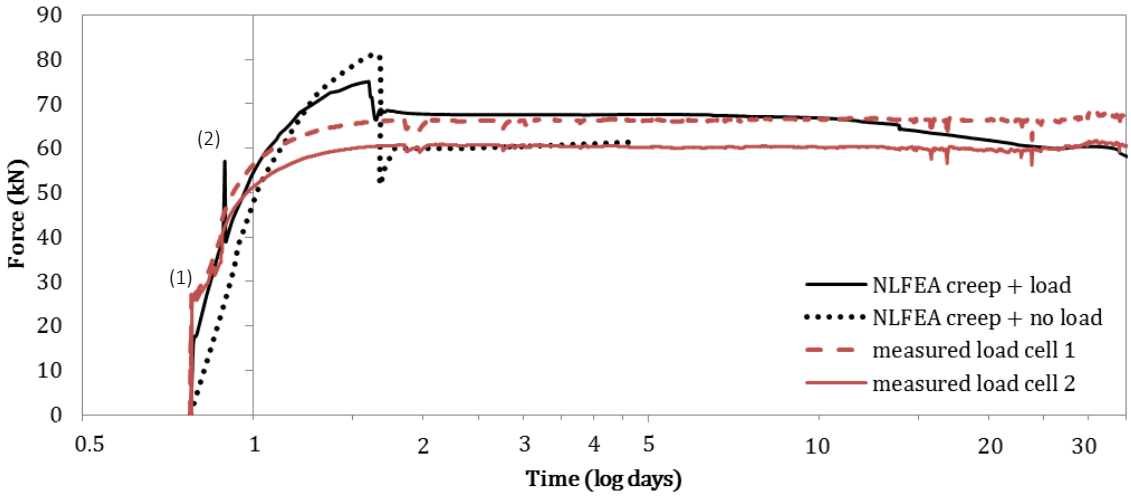

(Continued in next page…)

(…continued from previous page)

d)

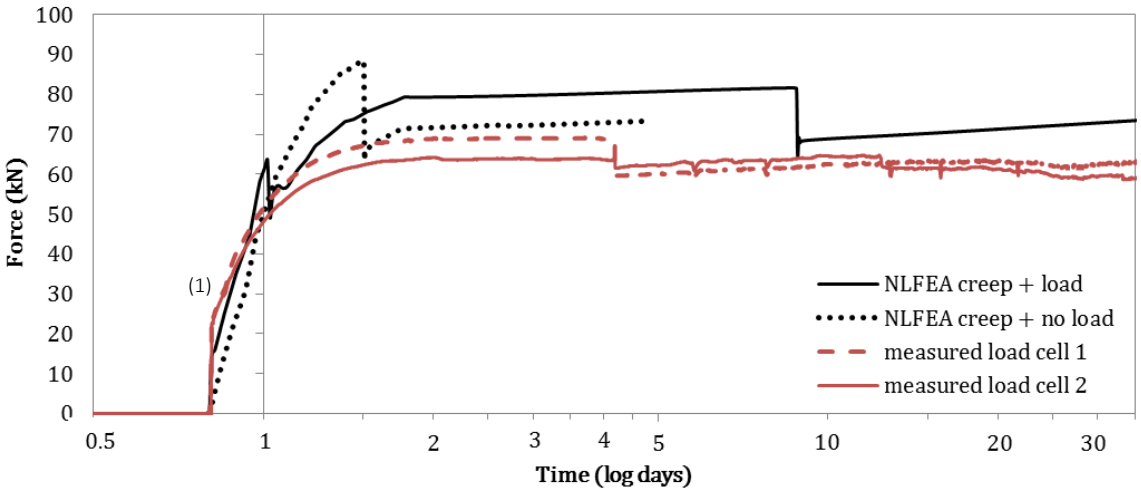

(1) – first actuator loading
(2) – second actuator loading

Figure 10: Measured and predicted load cell reactions in: a) E-W1; b) E-W2; c) E-W3; and d) E-W4

Table 2 shows the stage 1 and 2 actuator loads and load cell readings immediately before and after unloading the actuators. The peak actuator loads, which are not shown in Figures 10 and 11, are seen to be less than the LT reactions. From Table 2, it can be deduced that during cooling to ambient, the preloads introduced into the walls with actuators were 12 kN in E-W1 out of a total of 97 kN (12%), 49 kN in E-W2 out of 103 kN (48%), 33 kN in E-W3 out of 62 kN (53%) and 23 kN in E-W4 out of 66 kN (35%).

The influence of stage 2 loading on the load cell reactions at first cooling to ambient can be seen by comparing reactions in walls E-W1 and E-W2 without and with stage 2 loading during cooling (Figure 11a). Walls E-W1 and E-W2 were geometrically identical and had the same reinforcement. The load cell reactions in both walls were around 100 kN at 45 hours, immediately before stage 2 loading was applied to E-W1 despite the preload being 12 kN in wall E-W1 and 47 kN in E-W2. Similarly, the load cell reactions in walls E-W3 and E-W4, with and without stage 2 loading, were similar at 62 kN and 66 kN respectively after cooling to ambient. The temperature drops to ambient were very similar in each pair of walls as shown in Figure 8a. Figures 11a and b show that the measured load cell reactions developed

at similar rates in each pair of walls, despite the difference in preload, with stage 2 loading having minimal effect on the final reactions. Note that Figure 11 does not show the stage 1 and 2 actuator loads listed in Table 2 or the corresponding change in load cell reactions. The increase of load cell reaction due to cooling was less in E-W2 than E-W1 which remained uncracked during cooling. Similarly, the increase of load cell reaction due to cooling was less in E-W3, which cracked under stage 2 loading, than E-W4 without stage 2 loading. Despite this, the final load cell reactions after cooling were very similar in each pair of walls. This suggests that the effect of increasing preload is counterbalanced by the reduction in stiffness that occurs upon cracking. Support for this is provided by the reduction in load cell reactions, visible in Figure 10 that occurred in E-W2 and E-W4 at 5.6 and 4 days respectively due to the formation of new cracks.

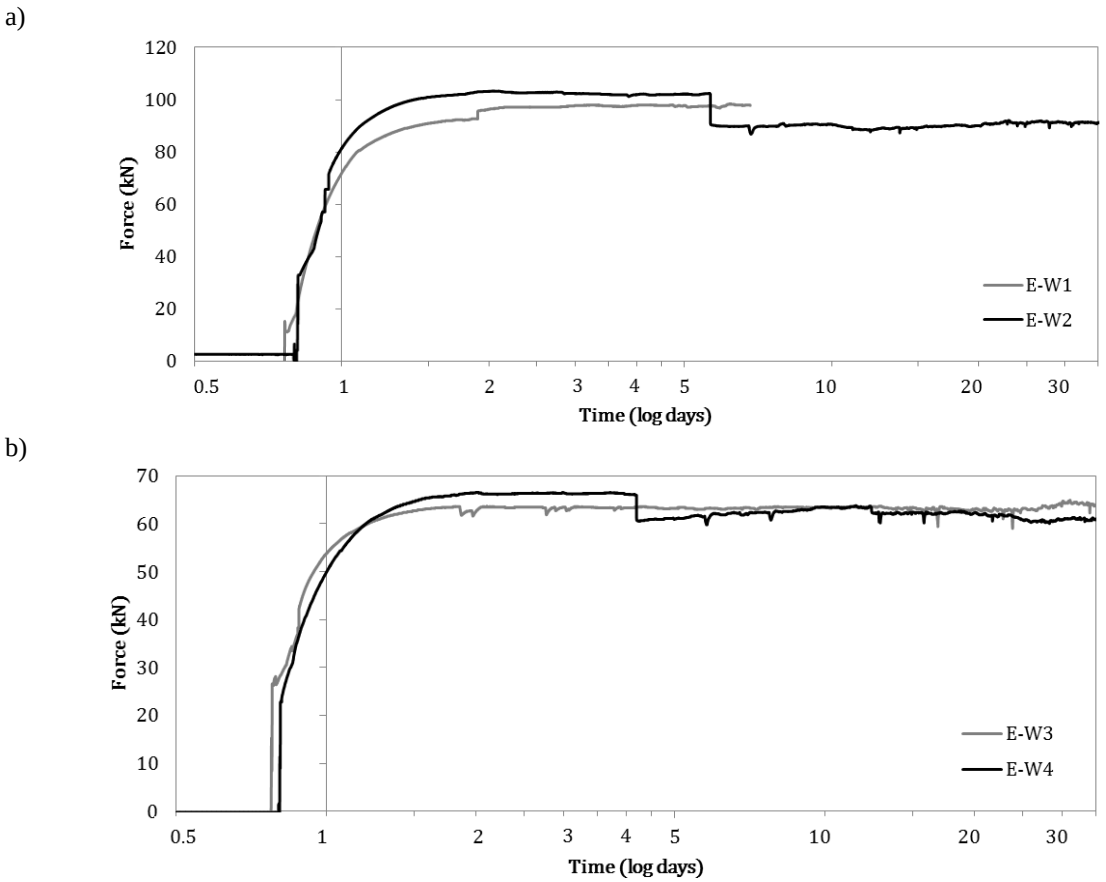

Figure 11: Comparison of development of load cell reactions with time in a) E-W1 and E-W2; and b) E-W3 and E-W4

Figure 10 also shows the load cell reactions predicted by NLFEA using the time-dependent concrete model (denoted "creep"). Results are shown without and with stage 1 and 2 preload. The reactions after two days are seen to be similar which is consistent with the comparison of reactions for wall pairs E-W1/E-W2 and E-W3/E-W4 in Figures 11a and b. Figure 12 compares the measured and "creep" NLFEA displacements at the load cells and end restraints from immediately before stage 1 loading. The NLFEA displacements at the load cells were imposed whereas those at the wall ends depend on the stiffness of the wall and end restraints.

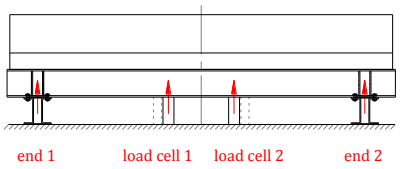

a)

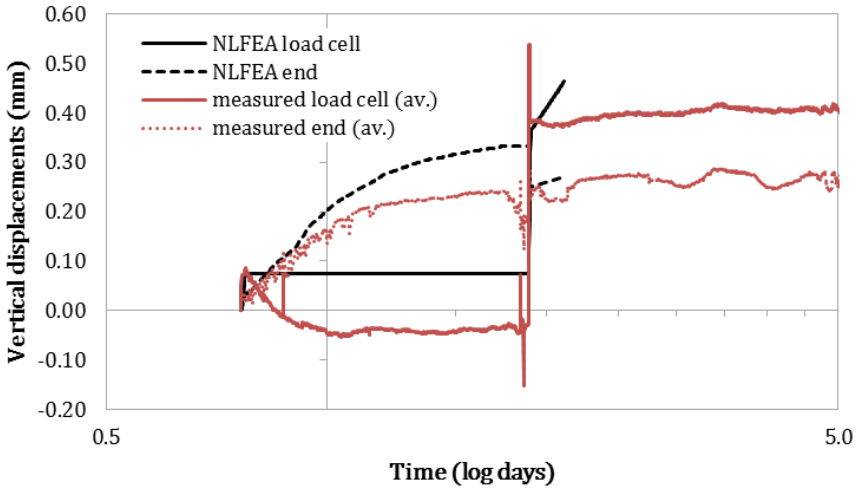

b)

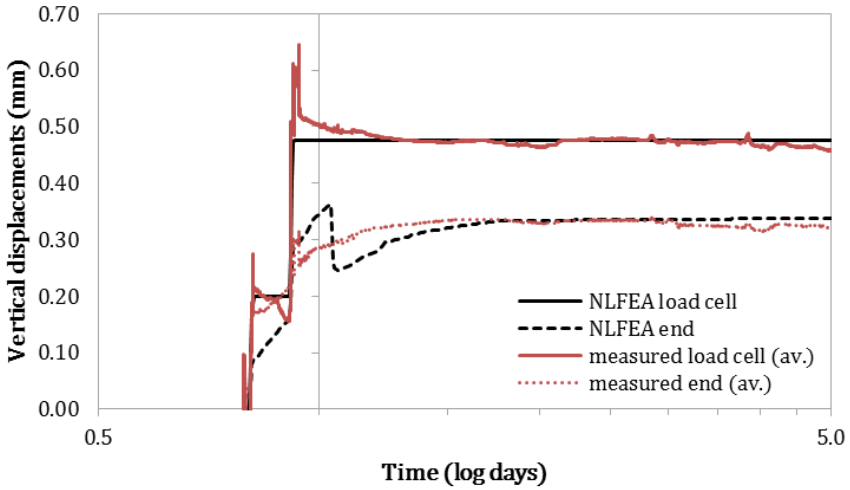

(Continued in next page…)

(…continued from previous page)

c)

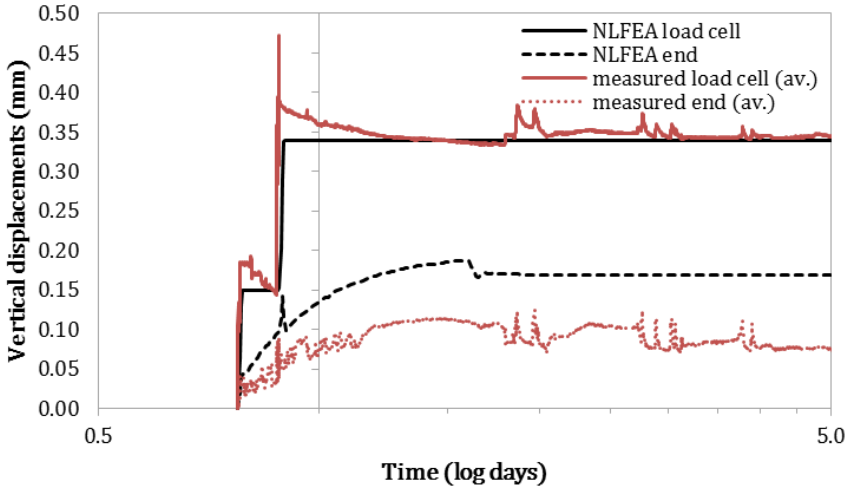

d)

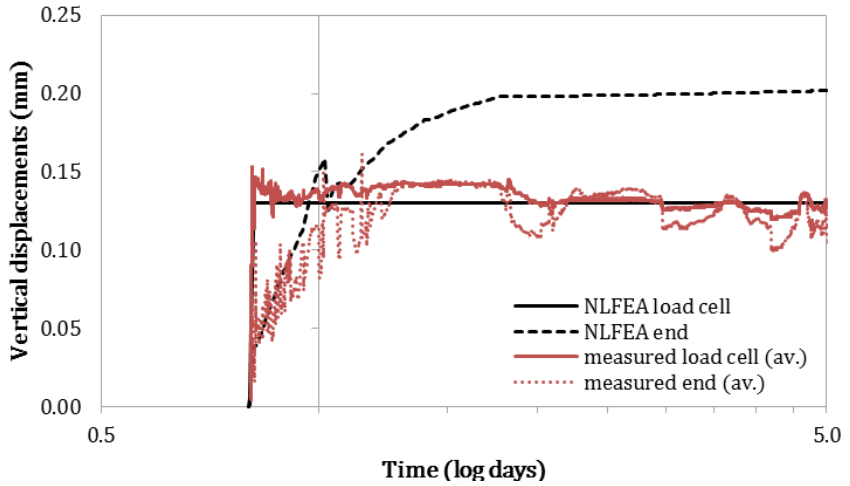

Figure 12: Vertical displacements of UC at centreline of end supports and at load cells in: a) E-W1; b) E-W2; c) E-W3; and d) E-W4

4.1 EAT and LT cracking

Figure 13 shows the crack pattern and crack widths in both faces of all walls. Cracks are shown in E-W1 at one week immediately before the wall was removed from the loading frame. The other crack patterns are shown immediately before final loading at around six weeks which was just before final loading of E-W3 and E-W4. Subsequently, further restraint induced cracks developed in E-W2 which was loaded later. A unique reference number is assigned to every crack in which the number refers to the week in which the crack formed and the letter to the sequence of crack formation within that week. Through cracks have the

same reference number on each face if the crack appeared on both faces of the wall in the same week. Wide cracks, shown in red, are depicted as primary and hairline cracks, shown in black, as secondary. With the exception of E-W1, the first cracks formed near the centre of the wall within 24 hours of the formwork being removed with more cracks forming in subsequent weeks. Stage 2 loading initiated crack 1a in wall E-W1, cracks 1a and 1b in E-W2 and cracks 1a, 1b and 1c in E-W3. All cracks in E-W4, with only stage 1 loading, developed subsequent to preloading the wall. Figure 13 shows that crack widths in E-W3 and E-W4, but not E-W1 and E-W2, were narrowest at the base of the wall and increased with height from the base as observed by Stoffers [2] in walls constrained to remain straight with aspect ratios of 6.7 and 8.

Maximum measured crack widths at EA (3 days) and LT (6 weeks) are presented in Table 4 which also notes the cracks which had formed at 3 days. Figure 14 compares the measured and predicted increase in crack width with time of the three widest cracks in walls E-W2, E-W3 and E-W4. The NLFEA predictions in Figure 14 include stage 1 and 2 loading. The initial crack widths after second stage loading of E-W2 and E-W3 are shown by the first plotted points in Figure 14a and b. Crack widths increased with time due to thermal contraction and shrinkage. The widest measured LT cracks formed in the first week. Subsequent shrinkage induced cracks were considerably narrower and are depicted secondary in Figure 13. With the formation of new cracks, existing cracks narrowed and then widened again with increasing shrinkage. The insets to Figure 14 also show the crack patterns that developed in the NLFEA with stage 1 and 2 loading. The primary cracks are mainly captured but not the narrower secondary cracks. The “no creep” NLFEA models give the best predictions of the maximum LT crack widths (see Table 4 and Figure 14) with the “creep + load” analysis giving crack widths closer to the mean of the primary crack widths plotted in Figure 14. It is concluded that NLFEA without creep and time-independent concrete

properties can give reasonable estimates of LT crack widths in base-restrained walls as previously found by Kianoush et al. [22]. The NLFEA gives better predictions of restraint induced crack width than spacing. The reason for this is that the crack width depends on the reinforcement stress at the crack and the slip of the reinforcement relative to the concrete to either side of the crack which appears to be reasonably captured in the NLFEA. The NLFEA broadly captures the primary cracks but not the secondary cracks, the simulation of which requires a more sophisticated, and probably three-dimensional, modelling approach.

a)

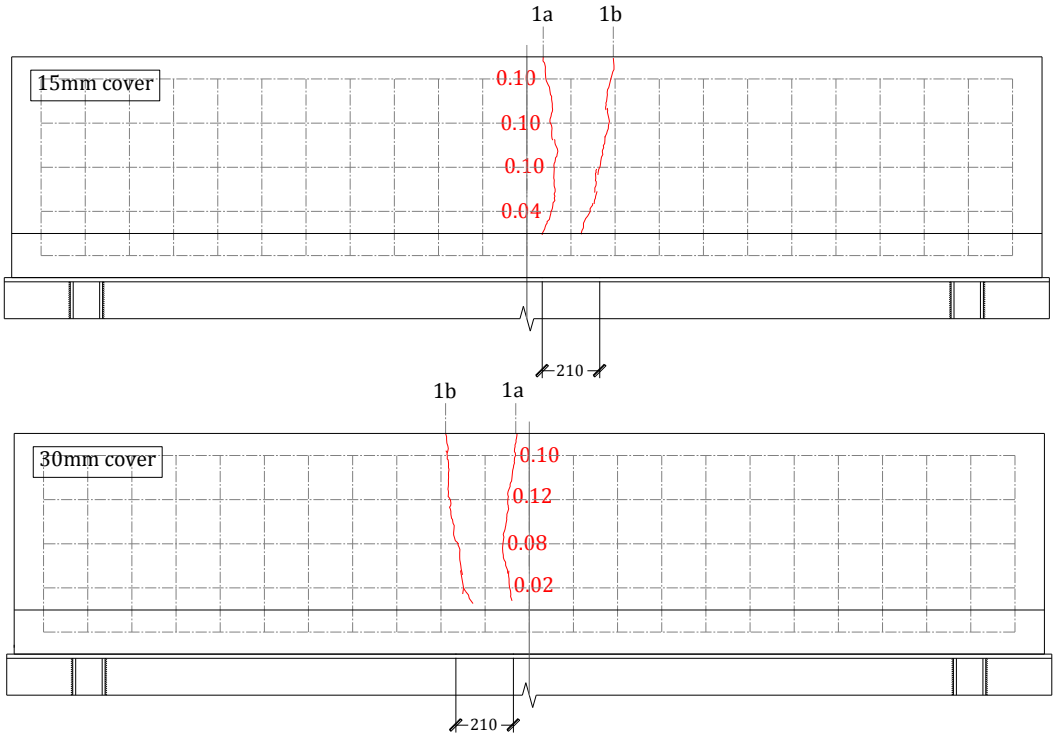

b)

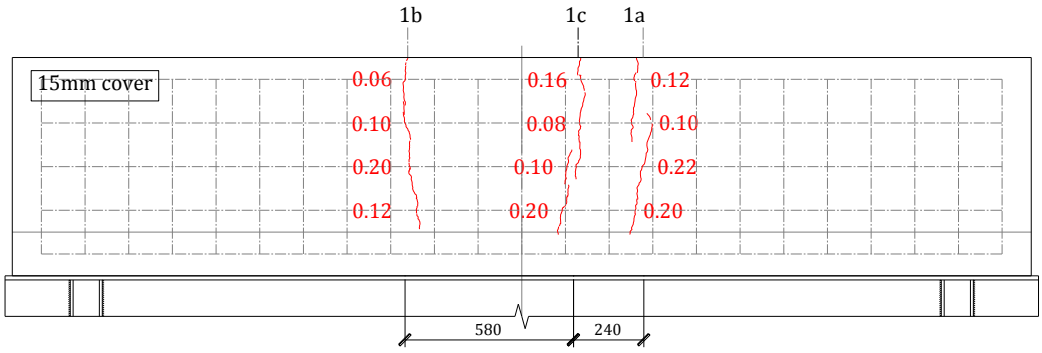

(Continued in next page…)

(…continued from previous page)

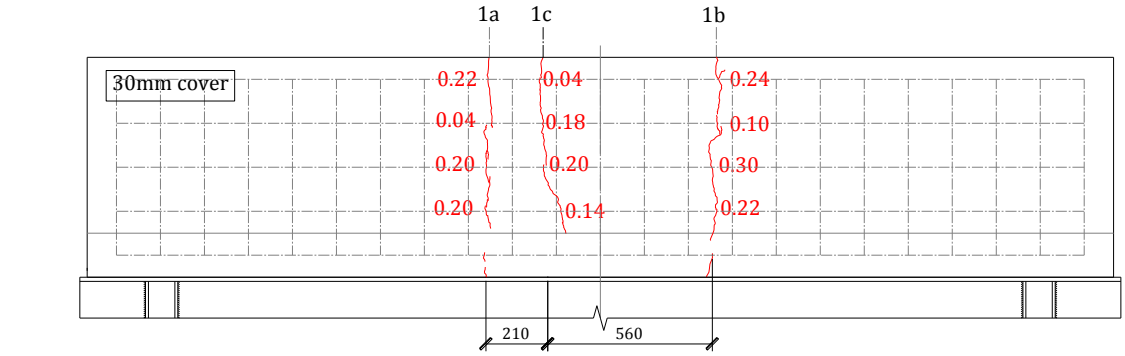

c)

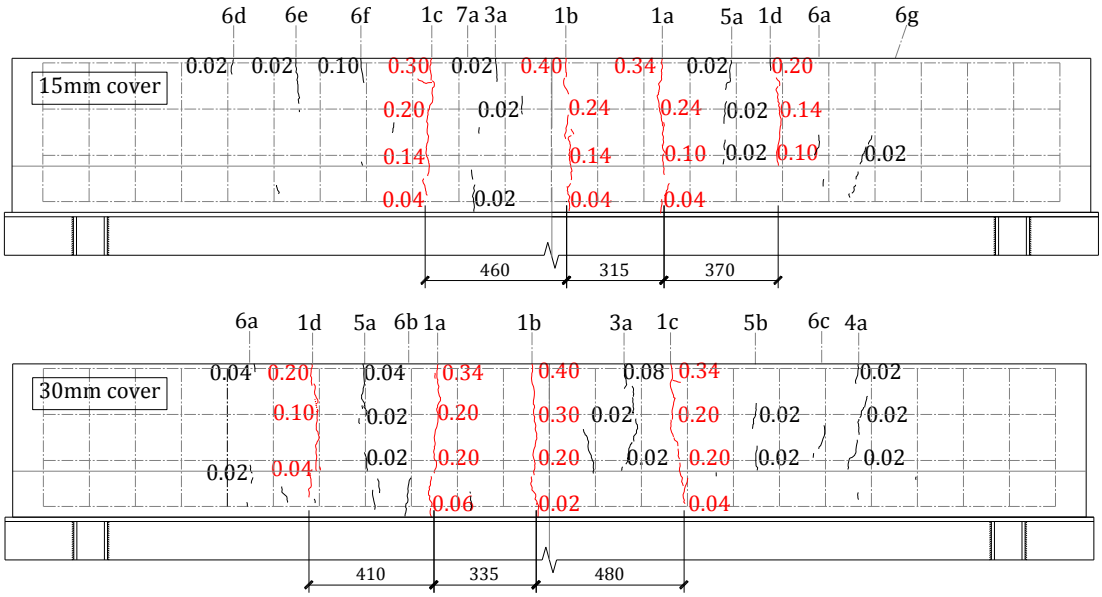

d)

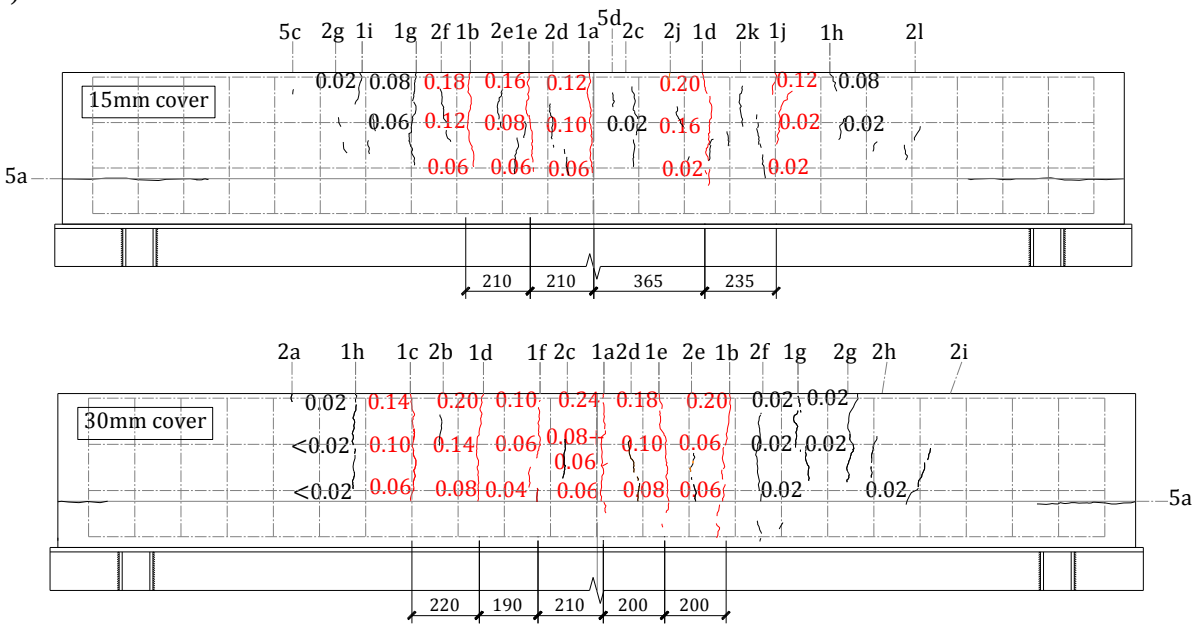

Figure 13: Crack patterns and widths: a) after 1 week in E-W1and after 6 weeks in b) E-W2; c) E-W3; and d) E-W4

Table 4: Measured and predicted crack widths and crack spacings in tested walls

	wall notation							
	E-W1		**E-W2**		**E-W3**		**E-W4**	
bar diameter ∅ [mm]	12		12		12		12	
number of horizontal bars per face	4		4		3		5	
wall height H including kicker [mm]	750		750		500		500	
horizontal reinforcement ratio $\rho = A_s/A_c$	0.67 %		0.67 %		0.75 %		1.26 %	
$\emptyset/\rho$ [mm]	1790		1790		1592		955	
maximum restraint at EA[1]	0.31		0.59		0.63		0.69	
maximum restraint at LT[2]	n/a		0.69		0.78		0.80	
EA free thermal strain [με]	522		470		400		400	
LT free strain [με]	802		750		680		680	
$\Delta\varepsilon_{max}$ [με] equation (3)	31		62		71		47	
cover c [mm]	15	30	15	30	15	30	15	25
EA (3 days) maximum crack width [mm]								
cracks at 3 days	1a, b	1a, b	1a,b	1a,b	1a-d	1a-d	1a,b,d	1a-d
observed	0.10	0.12	0.20	0.22	0.20	0.22	0.12	0.12
NLFEA (creep + no load)	no cracks		no cracks		0.19		0.13	
NLFEA (creep + load)	n/a*		0.27		0.17		0.15	
LT (6 weeks) maximum crack widths [mm]								
observed	n/a#	n/a#	0.22	0.30	0.40	0.40	0.20	0.24
NLFEA (no creep + no load)	n/a		0.33		0.46		0.28	
NLFEA (no creep + load)	n/a*		0.59		0.43		0.28	
NLFEA (creep + load)	n/a*		0.30		0.23		0.13	
measured final crack spacing after loading [mm]								
$2s_{\min}$	n/a*		314		354		188	
s_{max}	n/a*		300		304		200	
$1.7s_{av}$	n/a*		371		364		244	
average maximum crack spacing[3]	n/a*		328		340		211	
EA $s = w_{max}/\varepsilon_R$	662		659		687		374	
LT $s = w_{max}/\varepsilon_R$	n/a		569		743		440	

[1] Measured after 2 days
[2] Measured at 6 weeks
[3] Average of the values for $2s_{min}$, s_{max} and $1.7s_{av}$
The boundary conditions of wall E-W1were changed because it was removed from the test setup after 7 days
* Wall E-W1 cracked under loading at ambient temperature and was removed from the loading rig after 1 week

a)

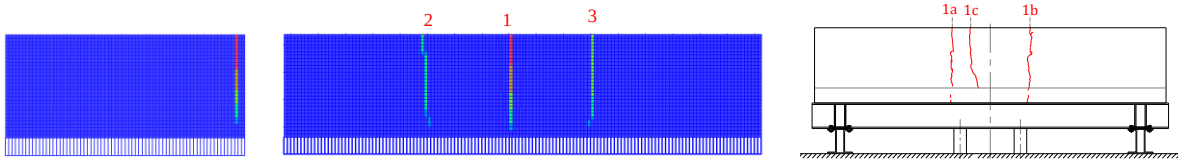

NLFEA (creep) at week 6 NLFEA (no creep) at an equivalent strain of week 6 experiment week 6 (30 mm cover face)

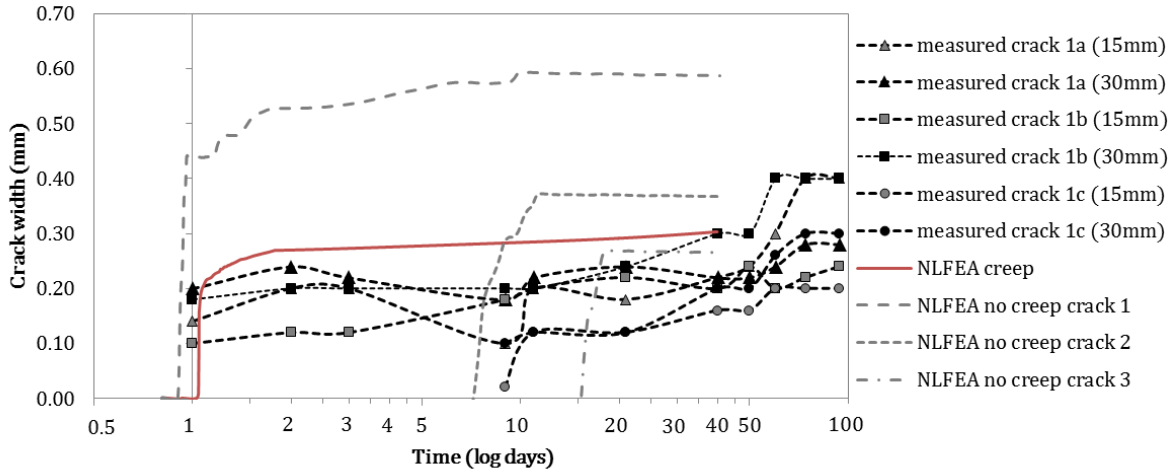

b)

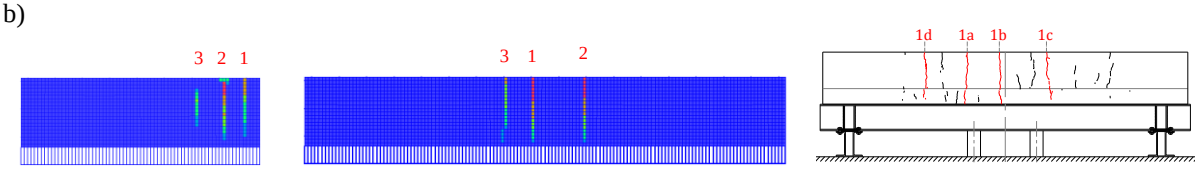

NLFEA (creep) at week 6 NLFEA (no creep) at an equivalent strain of week 6 experiment week 6 (30 mm cover face)

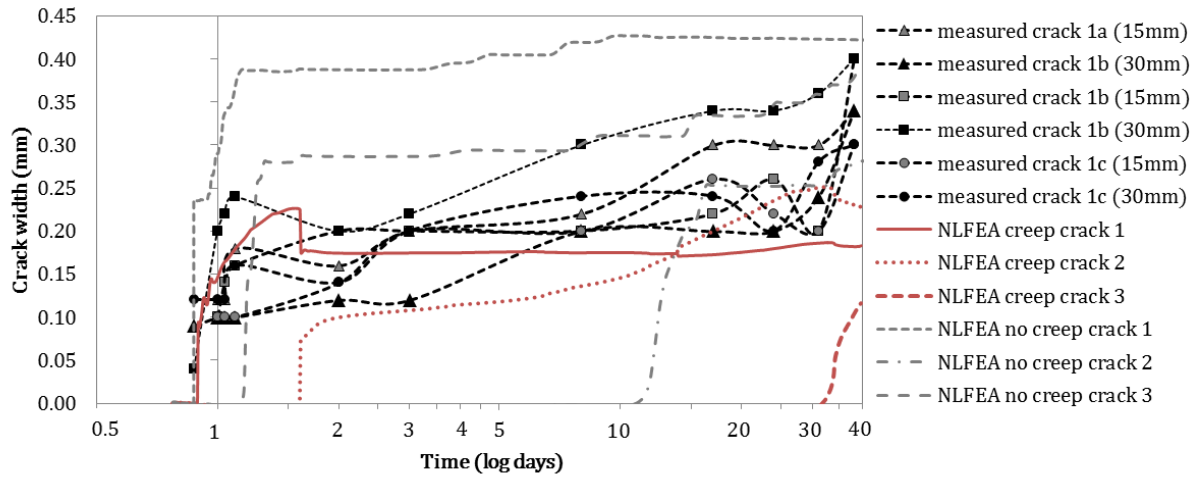

(Continued in next page…)

(…continued from previous page)

c)

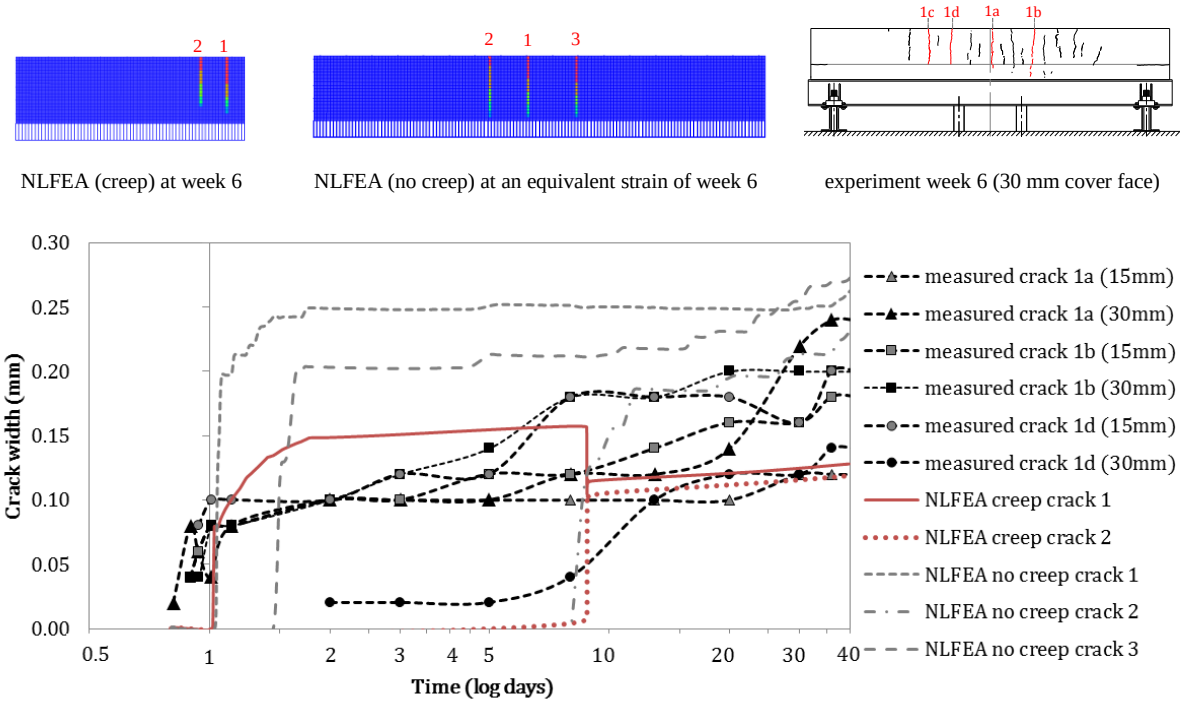

Figure 14: Comparison of measured and NLFEA predicted crack width variation with time for primary cracks in: a) E-W2; b) E-W3; and c) E-W4

a)

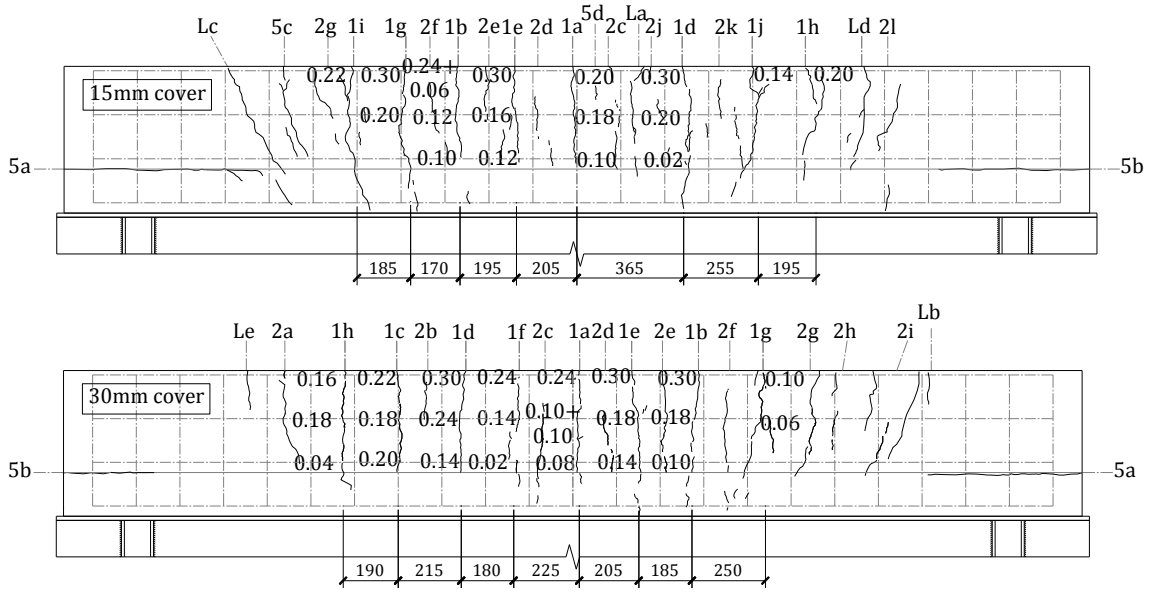

b)

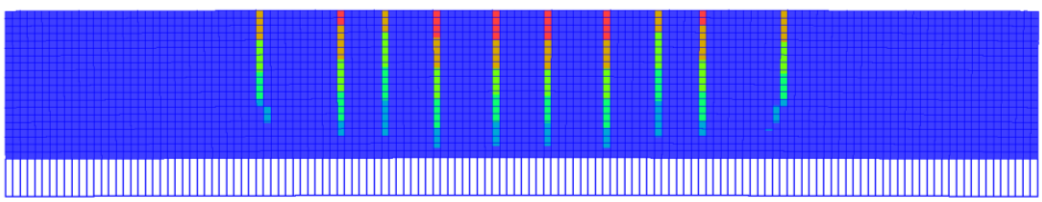

Figure 15: Crack patterns in E-W4 after loading each load cell to 200 kN: a) measured; and b) predicted

4.2 Comparative assessment

Crack widths in edge-restrained walls are calculated in EN 1992-3 [13] as the product of the design crack spacing and restrained strain $R\varepsilon_{free}$. Since reinforcement was detailed similarly to retaining walls, the cover to the horizontal reinforcement differed on each face. The effect of this on the measured crack spacing in each face and maximum crack width was minimal. On the other hand, the reinforcement ratio had a significant effect on the observed crack spacing and width with both least in wall E-W4, which was most heavily reinforced.

Horizontal restraint factors were calculated for each wall with equation (1) from DEMEC strains assuming that the free strain could be approximated as the measured vertical DEMEC strain. Restraint was greatest in the central third of the wall and reduced towards the ends. Table 5 shows the variation in mean EA restraint factors R with height over the central 1200 mm of each wall. The corresponding maximum EA and LT restraint factors R are listed in Table 4. The restraint factors increased with time due to the reduction in wall stiffness due to cracking. Notably, the maximum restraint factors are greatest for walls E-W3 and E-W4 with the highest aspect ratio.

Table 5: EA average horizontal restraint (over the central 1200 mm) at the end of day 2

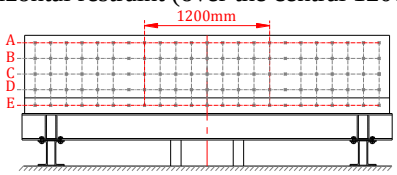

gridline*	E-W1	E-W2	E-W3	E-W4
A-B	0.02	0.41	0.59	0.69
B-C	0.31	0.56	0.63	0.65
C-D	0.25	0.53	0.48 (k)	0.48 (k)
D-E	0.17 (k)	0.59 (k)	n/a	n/a

* restraint is calculated midway between pairs of horizontal gridlines
(k) indicates restraint at kicker

Figure 16 shows the variation in mean restrained strain over the central 1200 mm of each wall, with height from the top flange of the UC at EA and LT. To compensate for the strain induced by stage 1 loading, which was not measured, the restrained strain was calculated as $\varepsilon_R = R\varepsilon_{free} + \Delta\varepsilon_r$ where:

$$\Delta\varepsilon_r = \frac{\delta}{0.84} y \times 10^6 \text{ με (tensile)} \qquad \text{(equation 3)}$$

in which δ (in mm) is the deflection at the load cells under stage 1 loading and y (in mm) is measured vertically (upwards positive) from the neutral axis of an uncracked transformed section consisting of the wall and UC. The stage 2 deflection is not included in δ since its effect is already included in the calculated restraint factor R. The coefficient of 0.84 in equation (3) is obtained from structural analysis using the second curvature area theorem.

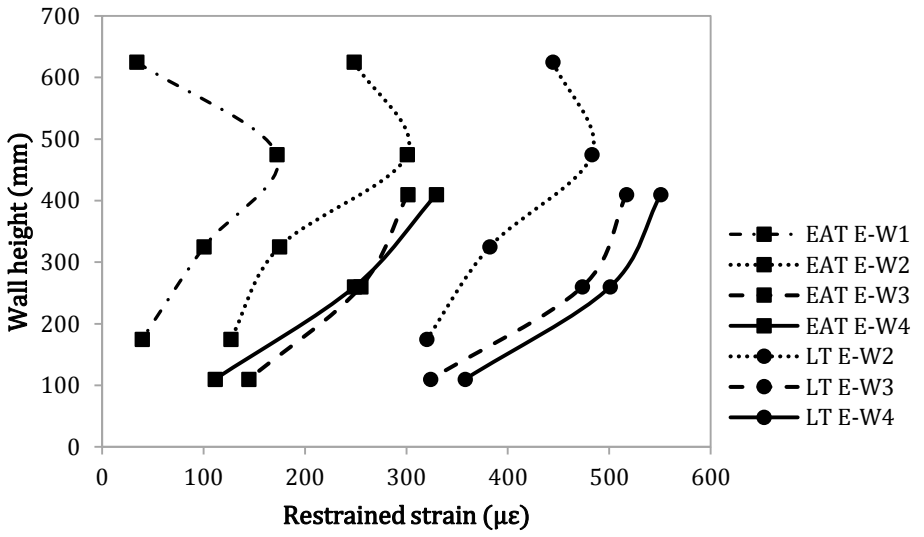

Figure 16: Variation in EAT and LT (week 6) restrained strain over wall height of tested walls

Stage 1 loading, which was insufficient to cause cracking, introduced vertical deflections of around 0.05 mm in E-W1, 0.10 mm in E-W2, 0.15 mm in E-W3 and 0.10 mm in E-W4. The extreme fibre strains $\Delta\varepsilon_{max}$ corresponding to these deflections are relatively small compared with the EA and LT free strains as shown in Table 4.

The relationship between crack width and restrained strain was investigated by dividing the maximum crack width by the mean restrained strain at that level from Figure 16. Significantly, the resulting crack spacings are significantly greater than the experimentally derived maximum spacings listed in Table 4 indicating that the product of restrained strain and maximum developed crack spacing is not a good indicator of maximum crack width contrary to the recommendations of EN 1992. This is so at EA because the crack pattern is undeveloped. The explanation in the LT, when the crack pattern is largely developed, is that the widths of later age cracks are significantly less than those of EA cracks (see Figure 13) as also found by Al Rawi and Kheder [3]. This is also consistent with the NLFEA where reasonable estimates of maximum crack widths were obtained even though not all the observed cracks were predicted to form. Figure 15 shows that the difference in width of EA and subsequent cracks largely disappears after loading to 200 kN.

5. Parametric studies

5.1 Model description

The experimental results suggest that crack widths are influenced by wall aspect ratio as well as reinforcement arrangement both of which were further investigated in a series of NLFEA parametric studies. Concrete was modelled with con9 which neglects creep, and time-dependent changes in concrete strength and stiffness, since this gives better predictions of LT crack widths than analysis with con12 which includes creep (see Figure 14). Further justification, is provided by Kianoush et al. [22] who also used NLFEA with 28 day concrete properties and no creep to obtain reasonable estimates of LT restraint induced crack widths in RC walls.

5.2 Influence of wall geometry on crack widths

Six sets of edge-restrained RC walls, depicted 1-a to 1-d and 2-a to 2-b, were modelled with the material properties, cross-sectional geometry and reinforcement arrangements given in Tables 6a and b respectively. Walls in each set had the same cross-sectional dimensions and reinforcement arrangement but varying length. The aim was to study the relationship between maximum crack width and wall aspect ratio L/H for walls of varying height.

Table 6: Parametric studies description:
a) material properties; and b) geometrical and reinforcement arrangements

a)

material model	f_{ct} **[MPa]**	f_{yk} **[MPa]**	E_c **[GPa]**	G_f **[N/m]**	E_s **[GPa]**	ν	**applied thermal strain [με]**
no creep ("con9")	3.0	500	25	140	200	0.17	-420

b)

model set no.	**wall height [mm]**	**wall thickness [mm]**	**bar diameter ∅ [mm]**	**vertical bar spacing [mm]**	**horizontal bar spacing [mm]**	**horizontal steel area per face A_s [mm^2]**	**horizontal reinforcement ratio ρ [%]**	$\emptyset/\rho$ **[mm]**
1-a	500	180	12	200	100	565	1.26	955
1-b	500	360	12	200	100	565	0.63	1910
1-c	500	180	16	200	200	603	1.34	1194
1-d	500	180	16	200	100	1005	2.23	716
2-a	750	180	16	200	200	804	1.19	1343
2-b	1500	180	16	200	200	1608	1.19	1343

Wall sets 1-a to 1-e were 500 mm high, and either 180 mm or 360 mm thick, with aspect ratios L/H between 1 and 9. These walls were modelled using 25 mm square concrete flat shell elements. The heights of wall sets 2-a and 2-b, with thickness 180 mm and aspect ratio between 1 and 10, were 750 mm and 1500 mm respectively. For practicality, a 50 mm square

mesh was used for wall set 2-b because mesh sensitivity studies gave similar crack widths for 25 mm and 50 mm element sizes. Nodes at the base of all walls were restrained both vertically and horizontally.

a)

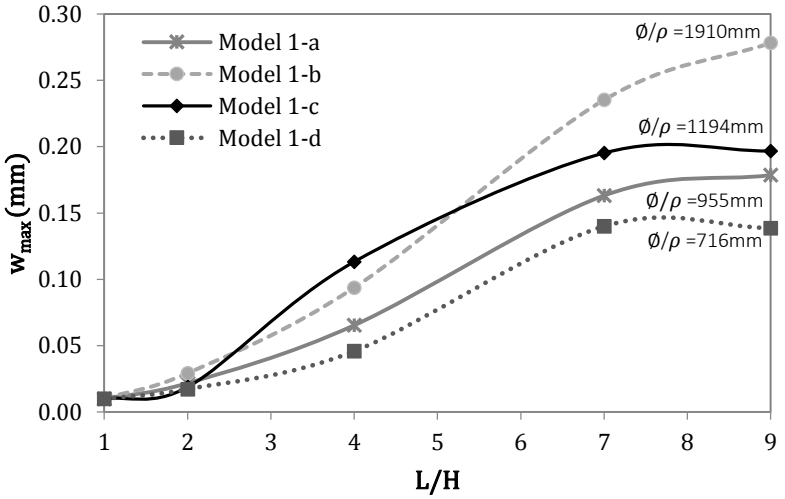

b)

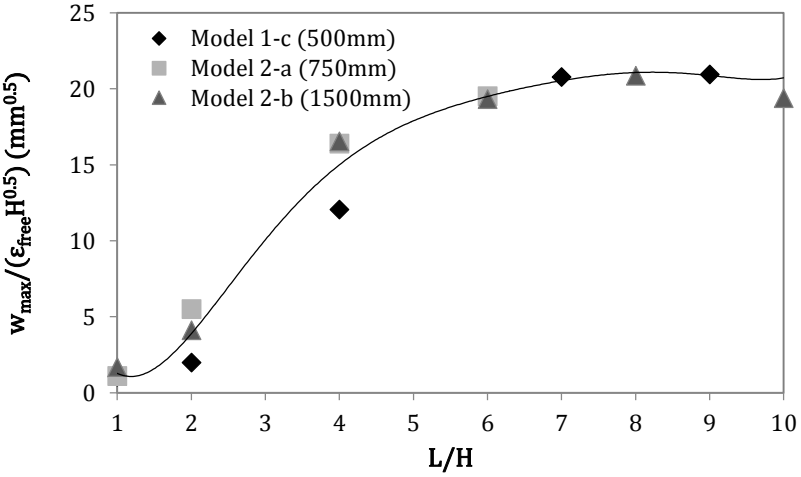

Figure 17: Parametric studies results showing the variation of: a) maximum crack widths with wall aspect ratio (H = 500 mm and varying Ø/ρ); and b) normalised maximum crack widths $w_{max}/(\varepsilon_{free}H^{0.5})$ with wall height (horizontal reinforcement H16-200 in each face)

The same compressive free strain of 420 με was applied uniformly to all walls. Figure 17a shows that the maximum crack widths in the 500 mm high edge-restrained walls depend on wall aspect ratio. Relatively small crack widths are predicted in walls with aspect ratios below 3 with significantly greater crack widths in walls with aspect ratios of 7-9. This is consistent with Kheder's change of restraint diagrams [5], which indicate a higher change of

restraint (and thus, greater crack widths) in walls of large aspect ratio. Figure 17a also shows that the maximum crack width for a given wall aspect ratio and imposed free strain increases with increasing ratio of bar diameter to reinforcement ratio $\emptyset/\rho$. Figure 17b, in which crack widths are normalised by dividing through by $\varepsilon_{free}H^{0.5}$, shows that crack widths in walls 1-c, 2-a and 2-b, with the same aspect ratio and horizontal reinforcement (H16-200), but varying heights *H* increase almost proportionally to $H^{0.5}$. This is consistent with the experimental observations of Stoffers [2] and Kheder [3-5] but contrary to the predictions of BS 8007 [11] and EN 1992 [12, 13] which relate crack width to the restraint factor which reduces with height from the base for $L/H < 8$ [23] whereas the observed crack widths increase with height (see Figure 13).

5.3 Influence of horizontal reinforcement arrangement on crack widths

Results from the analyses of the previous section and additional NLFEA were used to investigate the influence of reinforcement arrangement on crack width for 500 mm high by 180 mm thick walls with aspect ratios of 4 and 7. The walls were reinforced with two layers of horizontal and vertical reinforcement. Vertical bars were 12 mm in diameter at 200 mm spacings. For each wall aspect ratio, eight horizontal reinforcement arrangements were modelled with bar spacings of either 100 mm or 200 mm and bar diameters varying between 12 mm and 32 mm. A temperature drop equivalent to a compressive strain of 420 $\mu\varepsilon$ was applied uniformly to each wall.

Figure 18 shows that the crack widths increase linearly with the ratio $\emptyset/\rho$ but also depend on the wall aspect ratio as shown in Figure 17a. BS 8007 [11] and EN 1992 [12, 13] also assume crack width increases linearly with $\emptyset/\rho$ but only account for the influence of wall geometry through the restraint factor which does not correlate with the increase in crack width with height from the base shown in Figure 13.

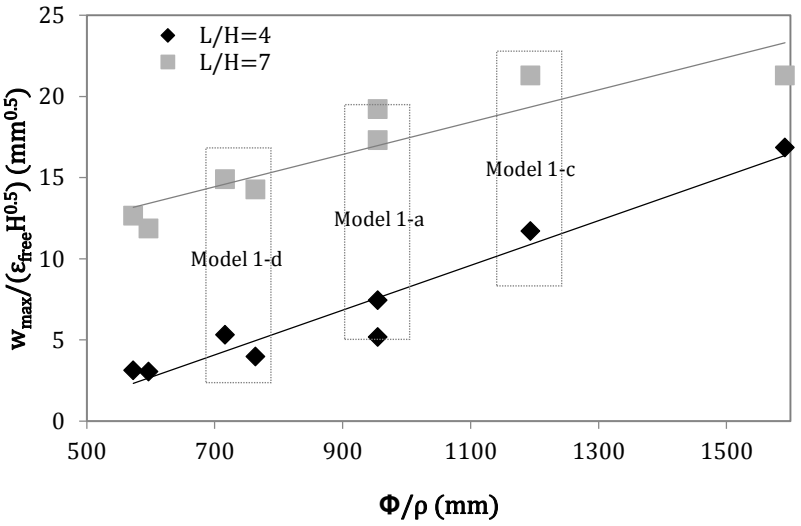

Figure 18: Parametric studies results showing the variation of normalised maximum crack widths $w_{max}/(\varepsilon_{free}H^{0.5})$ with $\emptyset/\rho$

6. Conclusions

This paper describes a research programme carried out to study EAT and LT cracking in RC edge-restrained walls subject to bending about their major axis. Results are presented for four test specimens with different reinforcement and geometric arrangements. The modelling of the tested walls with NLFEA is described, as are subsequent parametric studies conducted using the validated NLFEA models. The key conclusions of the research are as follows.

The first EA cracks, not directly caused by preload, developed in the central portion of the wall, where restraint was greatest. These cracks were primary cracks and remained widest throughout the monitoring period. Only horizontal cracks formed at the wall ends within lines drawn at 45° from the bottom corners. In the conducted tests, it was evident that increasing the reinforcement ratio decreased crack widths with the smallest crack widths observed in E-W4 with the highest horizontal reinforcement ratio.

The NLFEA without creep gives reasonable upper bound estimates of measured LT crack widths whereas the analysis with creep gives predictions closer to mean measured values. More accurate simulation of the development of cracking with time, and crack widths, would

require better modelling of concrete material properties, including tensile creep, but this is beyond the scope of the research. Both the test results and the NLFEA parametric studies show that crack widths in edge-restrained walls are significantly influenced by wall aspect ratio and height. Wider cracks were observed in wall E-W3 with aspect ratio 10 and ρ = 0.75 % than E-W1 and E-W2 with aspect ratio 5.8 and ρ = 0.67 %. This finding was reflected in the NLFEA results which also showed crack widths in walls with the same aspect ratio and horizontal reinforcement arrangement to increase with wall height. These findings are consistent with the experimental findings of other researchers [2-5]. NLFEA parametric studies indicate that crack widths in walls of the same aspect ratio and height increase linearly with the ratio of bar diameter to reinforcement ratio. However, further tests are required to study the influence of cover on crack spacing and width. The effect of cover could not be investigated in the 2D NLFEA presented in this paper.

Results presented in this paper are of significance because they highlight the importance of considering the influence of wall aspect ratio and height in design equations for crack widths in base-restrained walls. Significantly, neither BS8007 nor EN 1992 properly consider the effect of wall aspect ratio and height on crack spacing and width in base-restrained walls. Both codes predict crack widths to reduce near the top of base-restrained walls because the elastic restraint factor reduces with height from the base whereas in reality the maximum crack width in walls of high aspect ratio increases with height from the base in walls constrained to remain straight.

Acknowledgements

The authors would like to acknowledge the financial support of Laing O'Rourke for the research and the experimental work described in this paper, as well as the staff of the

Structures Laboratory at Imperial College London, in particular, Mr Leslie Clark, for their assistance with the tests.

References

[1] Gilbert RI. Time-dependent cracking and crack control in reinforced concrete structures. ACI Special Publication. 2005;225:223-44.
[2] Stoffers H. Cracking due to shrinkage and temperature variations in walls. Heron. 1978;23:1-A4.
[3] Al Rawi RS, Kheder GF. Control of cracking due to volume change in base-restrained concrete members. ACI Structural Journal. 1990;87:397-405.
[4] Kheder GF, Al Rawi RS, Al Dhahi JK. Study of the behavior of volume change cracking in base-restraint concrete walls. ACI Materials Journal. 1994;91:150-7.
[5] Kheder GF. A new look at the control of volume change cracking of base-restrained concrete walls. ACI Structural Journal. 1997;94:262-70.
[6] Beeby AW, Forth JP. Control of cracking in walls restrained along their base against early thermal movements. International Conference. University of Dundee, Scotland, UK: Thomas Telford, London; 2005. p. 123-32.
[7] Anson M, Rowlinson PM. Early-age strain and temperature measurements in concrete tank walls. Magazine of Concrete Research. 1988;40:216-26.
[8] Carlson RW, Reading TJ. Model study of shrinkage cracking in concrete building walls. ACI Structural Journal. 1988;85:395-404.
[9] Yamazaki M. Thermal cracking of a thick wall. Concrete International. 1986;8:44-8.
[10] Evans EP, Hughes BP. Shrinkage and thermal cracking in a reinforced concrete retaining wall. ICE Proceedings. 1968;39:111-25.
[11] BSI. BS 8007:1987 Code of practice for design of concrete structures for retaining aqueous liquids. BSI; 2008.
[12] BSI. BS EN 1992-1-1:2004 Eurocode 2 Design of concrete structures - Part 1-1: General rules and rules for buildings. BSI; 2011.
[13] BSI. BS EN 1992-3:2006 Eurocode 2 Design of concrete structures - Part 3: Liquid retaining and containment structures. BSI; 2006.
[14] Micallef M. Crack control in base-restrained reinforced concrete walls. London: Imperial College London; 2015.
[15] IStructE, Concrete Society. Standard method of detailing structural concrete - a manual for best practice. 3 ed: The Institute of Structual Engineers; 2006.
[16] Izzuddin BA. Nonlinear dynamic analysis of framed structures: Imperial College, University of London; 1991.
[17] Macorini L, Fragiacomo M, Amadio C, Izzuddin BA. Long-term analysis of steel–concrete composite beams: FE modelling for effective width evaluation. Engineering Structures. 2006;28:1110-21.
[18] CEB-FIP. CEB-FIP Model Code 1990. Lausanne, Switzerland: Comite Euro-International du Beton; 1998.
[19] Izzuddin BA. ADAPTIC user manual revision 1.4e. Imperial College, University of London: Department of Civil and Environmental Engineering; 2012.
[20] Kianoush M.R., Acarcan M., Ziari A., Behavior of base restrained reinforced concrete walls under volumetric change, Engineering Structures. 2008; 30:1526‑1534.

[21] Beeby A.W., Scott R.H., Mechanisms of long-term decay of tension stiffening, Magazine of Concrete Research. 2006; 58(05);255‑266.
[22] fib. Model Code for concrete structures 2010. Lausanne, Switzerland: fib; 2013.
[23] Vollum R.L., Afshar N., Izzuddin B.A., Modelling short-term tension stiffening in tension members, Magazine of Concrete Research. 2008; 60:291‑300.
[24] Bamforth PB. CIRIA C660 Early-age thermal crack control in concrete. 2014.
[25] Narayanan R.S., Beeby A.W., Designers' guide to EN1992-1-1 and EN1992-1-2: Design of concrete structures. General rules and rules for buildings and structural fire design, Thomas Telford Publishing, 2005.